NTNU
Norwegian University of
Science and Technology

Photoelectrochemical Characterization of Dye-sensitized Solar Cells

Niklas Aabel

Chemical Engineering and Biotechnology
Submission date: June 2018
Supervisor: Svein Sunde, IMA

Norwegian University of Science and Technology
Department of Materials Science and Engineering

NORWEGIAN UNIVERSITY OF SCIENCE AND TECHNOLOGY

DEPARTMENT OF MATERIALS SCIENCE AND ENGINEERING

MASTERS THESIS

Photoelectrochemical Characterization of Dye-sensitized Solar Cells

Author:
Niklas Aabel

Supervisor:
Prof. Svein Sunde

June 29, 2018

Summary

Dye-sensitized solar cells, DSSCs, are thin film solar cells based on a photoelectrochemical system where a photo-sensitized anode and an electrolyte forms a semiconductor. Upon exposure of sunlight, the surface of the DSSC absorbs the photon energy, exciting electrons to a higher energy state. The electron is then transferred into the conduction band of a semiconductor where it in turn diffuses to the anode and through an outer circuit.

The most commonly applied solar cell technology today is direct conversion to electricity in photovoltaic units. However, current photovoltaic systems are quite complex and resource demanding. DSSCs meet the requirement of sufficient energy demands and offer a simpler technology, making them a potential substitute for photovoltaic cells in the future. Vital for the performance of DSSCs is the choice of dye. Most commonly Ruthenium complexes are used as dyes, but Ruthenium is quite scarce and expensive resulting in an interest for organic dyes. In this work, the impact of three organic dyes, AFB-18, AFB-19 and AFB-21, on the kinetic properties of DSSCs are studied. The results are benchmarked against the extensively studied organo-metallic dye N719. Current-voltage-characteristics, electrochemical impedance spectroscopy, EIS, and intensity modulated photo-current spectroscopy, IMPS, are measurements used for analyzing the cell's properties. The current-voltage-characterisitics showed promise that pure organic dyes can compete with the commonly used Ruthenium complexes in terms of performance. The differences in the current-voltage-characteristics for the different solar cells are explained through the corresponding time constants for transport and recombination.

Preface

This report is a masters thesis carried out during the spring of 2018 as a part of the subject TMT4900 at NTNU. The work has been supervised by Prof. Svein Sunde, and consists of both experimental testing and mathematical programming. Characterization and interpretation has been done by the author, while construction of the solar cells was performed with the help of PhD candidate Audun Formo Buene at the Department of Chemistry.

Table of Contents

List of Tables

List of Figures

Chapter 1

Introduction

According to the Intertergovernmental Panel on Climate Change[13], the global energy demand in 2040 will be 28% higher than the current level. In addition, renewable energy sources must account for a substantially larger fraction of the global energy demand than today to meet the goals of the Paris Agreement of 2016. In order to meet this demand, new sources of energy must be utilized. Solar energy is one of the most promising renewable energy technologies, partly because it is easy to implement in large-scale energy systems, but also because the technical potential for solar energy is the highest among the renewable energy sources. Estimates for solar energys technical potential range from 1,575 to 49,837 EJ/yr, that is, roughly 3 to 100 times the worlds primary energy consumption in 2008.[13]

Preferably direct conversion to electricity in photovoltaics are utilized in solar cells, but current photovoltaic systems are quite complex and resource demanding.[2] Photo-electrochemical solar cells meet the requirements of sufficient energy demands and a simple technology. However, stability appears to dictate a band gap substantially larger ($>$ 3 eV) than optimum in terms of solar-to-electricity energy conversion[17][16]. Dye-sensitized solar cells, DSSCs, solves this stability vs efficiency problem as it separates the light absorption process and the charge separation process [3].

DSSCs are thin film solar cells based on a photoelectrochemical system where a photo-sensitized anode and an electrolyte forms a semiconductor. Upon exposure of sunlight the dye on the surface of the DSSC absorbs the photon energy, exciting electrons to a higher energy state. The electron is then transferred into the conduction band of a semiconductor where it in turn diffuses to the anode and through an outer circuit.

Traditional solar cells are made of ultra-pure semi-conductor materials, often silicon, providing a high cost due to high amounts of energy required for production. DSSCs may be a low-cost alternative to traditional solar cells. Most commonly Ruthenium complexes are used as dyes in DSSCs, but since Ruthenium is a costly, scarce and noble resource it is resulting in an interest for organic dyes. Organic dyes are associated with high flexibility, are simple to synthesize and contain elements that are cost-effective.

In this report I will study how the dye influences the kinetic properties of the DSSC. This is assessed by photoelectrochemical characterization methods for four different dyes.

The results for DSSCs with the three pure organic dyes AFB-18, AFB-19 and AFB-21 will be benchmarked against DSSCs with the well known organo-metallic dye N719, where the substrate will be a TiO_2 semi-conductor for all cells. The goal is to explain differences in the cells' current-voltage-characteristics through the corresponding time constants for transport and recombination. It is assumed that the transport is restricted to diffusion occurring in the semi-conductor, leading to a hypothesis that the time constant for transport is equal for all cells, and that the different dyes effect the recombination and hence determine the differences in the performance of the cells.

Chapter 2

Theory

2.1 Dye-sensitized solar cells

The operation of DSSCs is based on light-induced charge separation at an interface between a liquid redox electrolyte or a solid hole conductor and nanoparticles of a wide-band gap semiconductor oxide, most commonly TiO_2, that form a nanostructured nanoporous photoelectrode. At this interface a monolayer of dye absorbs photons and injects electrons to the conduction band of the TiO_2 particle, which is followed by transport of the electrons by diffusion through the nanoparticle film to the collecting contact [11].

When exposed to sunlight a dye on the surface of the DSSC absorbs photon energy, exciting electrons from its highest occupied molecular orbital, HOMO, into its lowest unoccupied molecular orbital, LUMO. The electron then gets transferred to the conduction band of a wide-gap semiconductor separating the charge separation process and the absorption process. The electron then transports through diffusion to an anode, forcing the electron through an outer circuit. At the counter electrode the electron reduces a red-ox couple in solution, which again ensures regeneration of the dye and closing the circuit. A simplified overview of how a dye-sensitized solar cell works can be seen in Figure 2.1

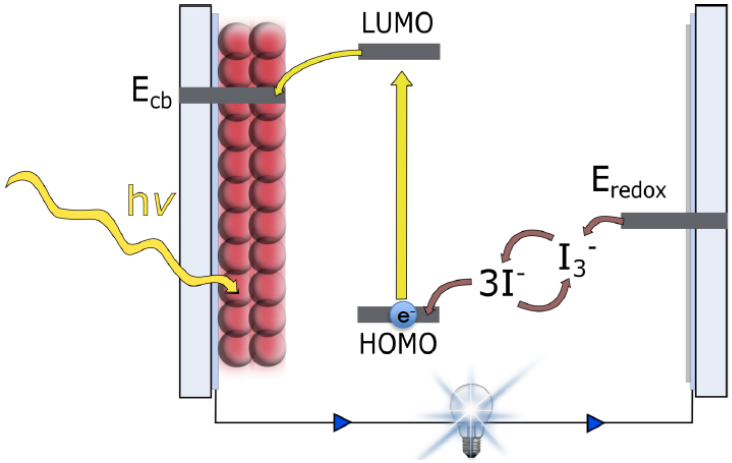

Figure 2.1: Simplified overview of how a dye-sensitized solar cell works. Figure made by PhD candidate Audun Buene.

For a semi-conductor stability and its relation to band gap can be expressed through Figure 2.2a[10]. From Figure 2.2b[10] it can be seen that TiO_2 fits scenario c in Figure 2.2a, making it susceptible to anodic photodecomposition.

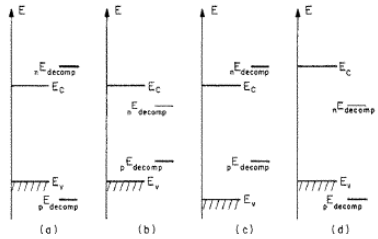

(a) Energy correlations between band edges and decomposition Fermi levels, characterizing susceptibility to photodecomposition. (a) Stable, (b) unstable, (c) susceptible to anodic photodecomposition, (d) susceptible to cathodic photodecomposition.

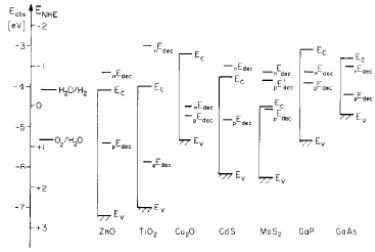

(b) Position of band edges and decomposition Fermi energies of various semiconductors and of water in absolute, E_{abs}, and electrochemical scale, E_{NHE}.

Figure 2.2: Both figures are taken from the article by Gerischer[10] referred to above.

S.R. Morrison concludes with an optimal band gap for solar-to-energy conversion being approximately $1.1eV$[17]. For band gaps lower than optimum, much of the photon energy absorbed is converted to heat as the charge carriers move to the band edges. For band gaps higher than optimum, the photon energy lower than the band gap are not absorbed. Since TiO_2 have a band gap of 3.2 eV[6], much of the photon energy from the illumination is not absorbed. The TiO_2 is therefore coated with a dye whose band gap is

closer to optimum. Since the light absorption process occurs in the dye whereas the charge separation occurs in the wide-gap semiconductor, both high stability and high efficiency can be obtained from a DSSC.

A conventional way of describing the performance of solar cells is the overall power conversion efficiency, PCE.

$$PCE = V_{oc} IscFF \tag{2.1}$$

where V_{oc} is the open circuit voltage, I_{sc} is the short circuit current, FF is the fill factor defined in equation (2.6). Through this relation it can be seen that the performance of the cell is increased with increasing V_{oc}, I_{sc} and FF. Generally V_{oc} can be increased by decreasing the recombination whereas a high I_{sc} is favored by a broad and strong absorption spectrum.

The efficiency is related to the transport and recombination in the semi-conductor. When an electron is injected into the conduction band of the semi-conductor it can either be collected or recombine. If the electron is transported to the TCO the electron is said to be collected, which is the desirable path for the electron. This transport is diffusion driven as the electrons are shielded from electrical fields. The shielding occurs due to the presence of a liquid electrolyte in a porous material, and hence drift is negligible. The accuracy of this approximation is demonstrated by Gentilini et al.[5] The average time it takes for an electron to diffuse through the TiO_2 and be collected is defined as the time constant for transport, τ_{trans} [15]. On the other hand if the injected electron reacts with the electrolyte, with the oxidized dye or simply de-excites, the electron is said to recombine. This is an undesired process, as the work of the electron cant be extracted. The average time an electron resides in the TiO_2 before recombining is defined as the time constant for recombination, τ_{rec}. In this work recombination with the electrolyte will be the dominating recombination as the oxidized dye is regenerated by the dye rapidly [1]. A schematic view over the processes occurring in a DSSC can be seen in Figure 2.3.

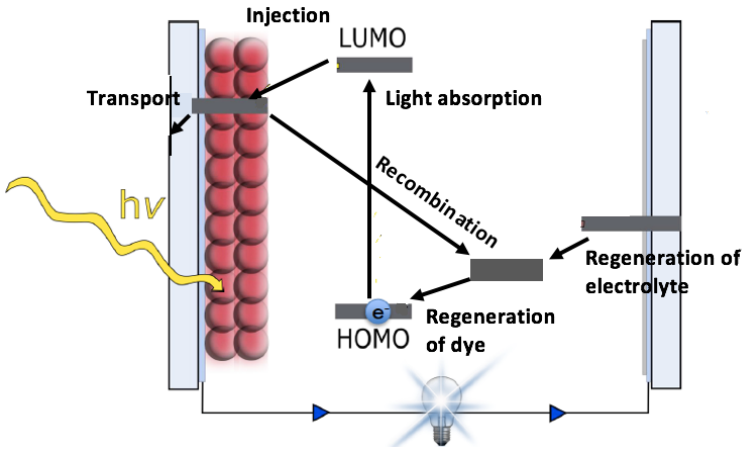

Figure 2.3: Schematic view over the processes occurring in a DSSC.

The two time constants for transport and recombination can be used to calculate the

charge-collection efficiency, η_{cc}, from the relation in equation (2.2). η_{cc} is a crucial factor for characterizing the overall performance of dye solar cells.

$$\eta_{cc} = 1\frac{\tau_{trans}}{\tau_{rec}}. \tag{2.2}$$

Generally the movement, transport and recombination at steady-state can be described by the following continuity equation[9]:

$$D''(x) - \frac{(n(x) - n_0)}{\tau} + \Phi\alpha e^{-\alpha x} = 0 \tag{2.3}$$

where D is the diffusion constant of electrons in the film, n(x) is the excess electron density, n_0 is the excess electron density in the dark, Φ is the incident light intensity, α is the reciprocal absorption length and τ is the mean charge carrier lifetime. The first term describes the diffusion movement, whereas the second and third term describes the recombination and generation respectively.

For a solar cell with diffusion length, L, larger than the film thickness, d, the photocurrent at the substrate electrode, J_{SE}, can be expressed as [9]

$$J_{SE} = J^0_{SE} - \frac{qDn_0d}{L^2}(e^{\frac{qV}{kTm}} - 1), \tag{2.4}$$

where J^0_{SE} is the measured current density, q is the charge on an electron, D is the diffusion constant, V is the potential, k is the Boltzmann constant is an ideality factor. Since $D/L^2 = 1/\tau_{rec}$, where τ_{rec} is the time constant for recombination, from equation 2.14, the photocurrent can be written as

$$J_{SE} = J^0_{SE} - \frac{qn_0d}{\tau_{rec}}(e^{\frac{qV}{kTm}} - 1). \tag{2.5}$$

In this study DSSCs consisting of glass plates, transparent conducting oxides, TCOs, TiO_2, dye monolayer, $I_3^-/3\,I^-$-electrolyte and platinum will be used, see Figure 2.4. In order to obtain as high efficiency as possible it is desirable to absorb as much sun light as possible and a fully transparent material, glass, is therefore used. This also applies for the TCO in addition to being conductive, ensuring electricity is able to flow. The TiO_2 is needed for stability of the system molecule which is obtained due to its high band gap of $3.2eV$[6]. A dye monolayer is stained on the surface of the TiO_2 lowering the band gap of the cell. The dye also absorbs the photon energy of the sun light in relation to its absorption spectrum. The electrolyte regenerates the dye whilst the platinum is used for catalyzing the cell.

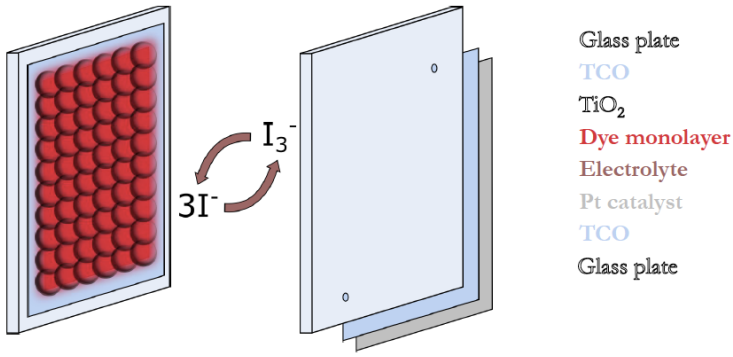

Figure 2.4: A simplified overview of how the dye-sensitized solar cell is built up. Figure made by PhD candidate Audun Buene.

2.2 Dyes

The dye properties are vital for a DSSC. Firstly, since the dye is the material absorbing the photon energy from the sunlight, it needs to display a broad and strong absorption spectrum in the visible area and high infrared area in order to ensure a high I_{sc}. Secondly the dye needs a good anchoring group in order to attach strongly to the semi-conductor, TiO_2. Thirdly it is desirable to have the highest occupied molecular orbital, HOMO, and lowest unoccupied molecular orbital, LUMO located at different parts of the molecule. Preferably LUMO is located at the anchoring group whereas HOMO has another spatial position in order to enhance the performance of the cell; the photon energy gets absorbed by the dye, exciting an electron from HOMO. The charge is then transfered to LUMO before the excitation occurs. This transport is known as metal-to-ligand charge transfer, MLCT[1]. This reduces the recombination, as the tunneling distances for recombination back to the HOMO of the dye are decidedly longer than for charge injection from the LUMO, meaning that the injection is kinetically favored. Figure 2.5 helps explain how the metal-to-ligand charge transfer occurs. Finally the dye should have LUMO slightly higher in energy than the conduction band of the semi-conductor in order to make the transport from the LUMO to the conduction band energetically beneficial.

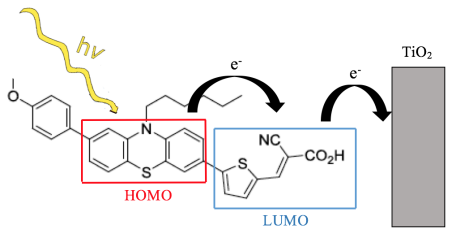

Figure 2.5: Incident light is absorbed by the dye, exciting electrons from HOMO to LUMO. Since HOMO and LUMO are at different locations in the molecule, the charge is transfered to the spatial position of LUMO before the excitation occurs. To complete the injection the charge is transported from LUMO of the dye to the conduction band of a semi-conductor. In this figure AFB5-182 is used as a dye and TiO_2 as a semi-conductor, but the same applies for other organic dyes and semi-conductors.

In this study four different dyes will be used: N719, AFB-18, AFB-19 and AFB-21. The N719 is a well known organo-metallic dye that has been extensively studied, which will be used as a reference dye. The molecular structure of N719 can be seen in Figure 2.6a. AFB-18, AFB-19 and AFB-21 are pure organic dyes and their molecular structures are displayed in figure 2.6b, 2.6c and 2.6d respectively.

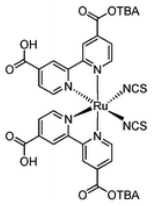

(a) Molecular structure of N719.

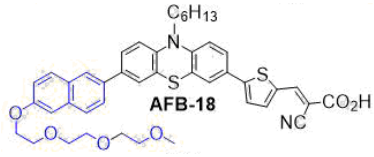

(b) Molecular structure of AFB-18.

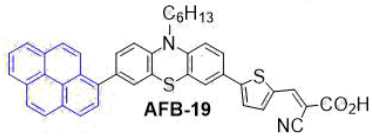

(c) Molecular structure of AFB-19.

(d) Molecular structure of AFB-21.

Figure 2.6: Molecular structures of the four dyes studied in this work.

The absorption specters of the four different dyes obtained by Audun Formo Buene can bee seen in Figure 2.7.

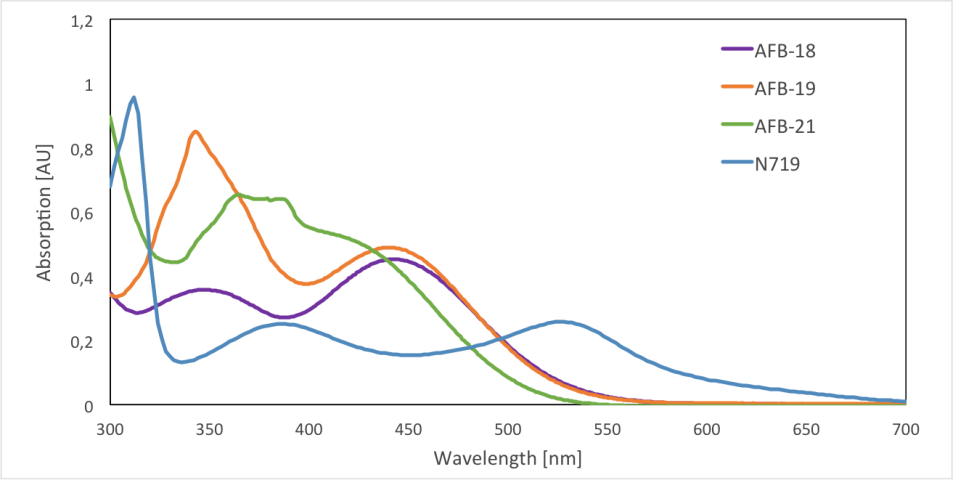

Figure 2.7: Absorption specters of the for different dyes - N719, AFB-18, AFB-19 and AFB-21. The sprectra are recorded in THF ($0.02mM$ concentration) with 1 cm light path.

2.3 Methods

Three different measurement techniques have been performed in this study. This section will explain both how they are measured experimentally and how the data can be interpreted.

2.3.1 Current-voltage characteristics

By measuring the current-voltage characteristics, IV-characteristics, the short circuit current, the open circuit potential and fill factor can be determined. During the measurement the light intensity is fixed at a constant intensity and wavelength while the current is measured as a function of the corresponding potential. The measurement can be performed at different sweep rates of the potential, but high sweep rates can result in dynamic effects occurring. The short circuit current is the current through the solar cell when the potential is zero, in other words when the cell is short circuited. Since the cell is experiencing the least resistive losses at short circuit, the short circuit current is the largest current the cell can obtain. The open circuit voltage is equivalently the potential across the cell at open circuit, meaning that the current is zero, and is hence the highest potential possible from the cell. The fill factor, FF, is defined as

$$FF = \frac{P_{max}}{I_{sc}V_{oc}}. \tag{2.6}$$

The fill factor is hence a measure of how close the output power of the cell is to its theoretical maximum. Increasing the shunt resistance, R_{sh} and decreasing the series resistance, R_s, in the cell increases the FF [18].

2.3.2 Electrochemical impedance spectroscopy

During electrochemical impedance spectroscopy, EIS, measurement a small amplitude sinusoidal voltage modulation $V_{CELL,AC}(\omega, t)$ is superimposed on a constant steady state cell voltage V_{CELL} and the resulting AC current density $i_{AC}(\omega, t)$ is recorded as a function of the modulation frequency, ω[11]. Figure 2.8 illustrates how EIS is measured, where the cell impedance, $Z_{CELL}(\omega)$, is defined as the ratio of the AC voltage and the current.

$$Z_{cell}(\omega) = \frac{V_{CELL,AC}(\omega, t)}{i_{AC}(\omega, t)} \tag{2.7}$$

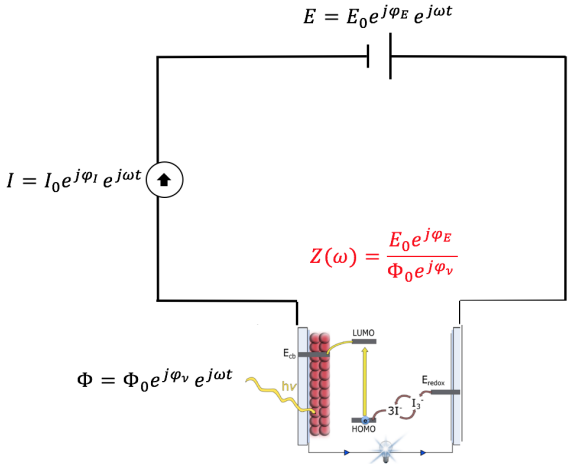

Figure 2.8: Figure showing how EIS is measured.

Halme et al.[11] derived the following expression for the impedance of a porous electrode by solving a continuity equation similar to equation (2.3):

$$Z_{TiO_2} = \frac{L}{Dc_\mu} \frac{1}{\sqrt{1 + (i\omega\tau)^{\beta_{CPE}}}} \coth\left(\frac{d}{L}\sqrt{1 + (i\omega\tau)^{\beta_{CPE}}}\right) \tag{2.8}$$

Where L is the diffusion length defined as $L = \sqrt{D\tau}$, D is the diffusion constant, d is the film thickness of the TiO_2, τ is the mean charge carrier lifetime, ω is the frequency, β_{CPE} is the constant phase element exponent and c_μ is the chemical capacitance defined as [11]

$$c_\mu = -\frac{\partial Q}{\partial V}. \tag{2.9}$$

For numerical solving of equation (2.8), equation (2.10), derived by Bisquert et al. [7], have been used. This is a modeled equation of the processes occurring in the TiO_2, to fit equation (2.8), where the number of variables are reduced to a set of minimum variables for solving. This is expected to be a good approximation at low frequencies.

The model used in this work is based on the equivalent circuit displayed in Figure 2.9 and accounts for the series resistance of the transparent conducting glass, R_s in addition to the impedance of the electron transport and of recombination in the TiO_2.

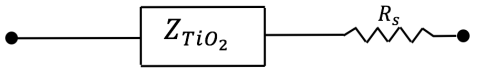

Figure 2.9: Equivalent circuit used for modeling the EIS. Z_{TiO_2} is the impedance of the electron transport and of recombination in the TiO_2 and R_s is the series resistance of the TCO.

$$Z = [\frac{R_1 R_3}{1 + (i\omega/\omega_3)^\beta}]^{1/2} \coth((\omega_3/\omega_L)^{\beta/2}[1 + (i\omega/\omega_3)^\beta]^{1/2}) \tag{2.10}$$

By comparing these equations the following relations can be found:

$$\frac{d}{L} = (\frac{\omega_3}{\omega_L})^{\beta/2} \tag{2.11}$$

$$\tau_{rec} = \frac{1}{\omega_3} \tag{2.12}$$

$$\tau_{trans} = \frac{1}{\omega_L} \tag{2.13}$$

$$D = \frac{L^2}{\tau_{rec}} \tag{2.14}$$

$$c_\mu = \frac{D}{L}(R_1 R_3)^{1/2} \tag{2.15}$$

The EIS-plots can be fitted with the use of equation (2.10). Hence the time constant for recombination, τ_{rec}, the time constant for transport, τ_{trans}, the diffusion constant, D, the chemical capacitance, Dc_μ and the diffusion length, L, can be found by using the above-mentioned relations in equation 2.11 through 2.15.

Further work ought to be expanded to a model that accounts for additional impedances occurring in the system, as done by Kern et al.[8]. This will expectedly provide more precise results than the model used in this work, as the it also takes into account the capacitance at the counter electrode, the bulk resistance and the electron transport in the electrolyte, described by Nernst diffusion. The model used by Kern et al. can be seen in Figure 2.10

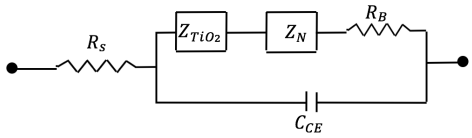

Figure 2.10: Expanded equivalent circuit used for modeling the EIS. Z_{TiO_2} is the impedance of the electron transport and of recombination in the TiO_2, Z_N is the electron transport in the electrolyte, R_s is the series resistance of the TCO, R_B is the bulk resistance and C_{CE} is the capacitance at the counter electrode.

For high efficiencies, the effective diffusion length, L, should be greater than the film thickness, d. This means that electrons can be efficiently collected at the electrode before they recombine [12].

Bisquert et al. [7] has shown that for EIS measurements, the shape of the impedance spectra is determined by the quotient

$$\frac{\omega_3}{\omega_L} = (\frac{R_1}{R_3})^{1/\beta}. \tag{2.16}$$

For $\omega_L > \omega_3$ it is obtained a linear line at high frequencies, and an arc at low frequencies, as shown in Figure 2.11b. The characteristic frequency, ω_L, is in this scenario located at the elbow, whereas ω_3 is located at the apex of the arc. For the other scenario, $\omega_3 > \omega_L$, the shape of the impedance spectra is shown in Figure 2.11c. In both figures ω_L and ω_3 are represented by a circle and a square, respectively.

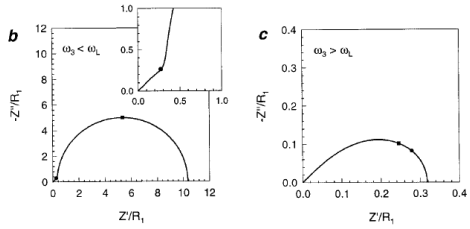

Figure 2.11: Above are the the two different shapes of the impedance spectra dependent on the relation between ω_L and ω_3 displayed. The frequencies corresponding to ω_L and ω_3 are represented by a circle and a sqaure, respectively

2.3.3 Intensity modulated photo-current spectroscopy

IMPS operate in a similar way as EIS, as seen in Figure 2.12. Instead of modulating the amplitude of the current or the potential, the light intensity is modulated. In IMPS the solar cell is held at constant voltage, potentiostatic control, and the AC current response $i_{CELL,AC}(\omega, t)$ caused by light intensity modulation is measured and correlated by the AC photon flux signal $\Sigma_{AC}(\omega, t)$ by defining the IMPS transfer function as

$$F_{IMPS,CELL}(\omega) = \frac{i_{CELL,AC}(\omega, t)}{q_e \Sigma_{AC}(\omega, t)} \tag{2.17}$$

where q_e is the electron charge [11].

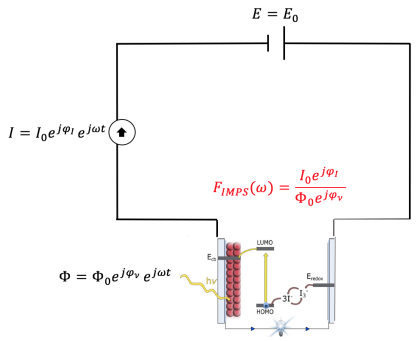

Figure 2.12: Figure showing how IMPS is measured.

The band gap between the valence band and the conduction band of the semiconductor is highest when the cell is short-circuited. As a result, nearly no electrons are injected into the conduction band. Most reactions occur on the back layer of the anode and electrons are migrating from the location where they are generated to the electrodes back layer. This electron transport time constant, τ_{trans}, can therefore be evaluated by IMPS through the following equation

$$\tau_{trans} = \frac{1}{2\pi * f_{IMPS}} \tag{2.18}$$

where f_{IMPS} is the specific frequency related to the electron transport [12].

At low potentials, electron transport is mainly restricted by diffusion through the electrodes active film with thickness, L. Electron recombination can therefore be neglected. Hence the electron diffusion coefficient can be calculated by [12]

$$D = \frac{d^2}{2.35 * \tau_{trans}}. \tag{2.19}$$

The relation between intensity modulated photo-current spectroscopy, electrochemical impedance spectroscopy and intensity modulated photovoltage spectroscopy, IMVS, can be expressed as

$$Z_{cell} = \frac{F^*_{IMPS,CELL}}{F^*_{IMVS,CELL}} \tag{2.20}$$

where the measurements of IMPS, IMVS and EIS are perfomed at the same conditions. IMVS is measured in the same way as IMPS, only galvanostatically at open circuit conditions. This means that a constant DC current is applied to the cell and the AC voltage response caused by light intensity modulation is measured and contrasted by the AC photon flux signal, giving the relation in equation (2.21)

$$F_{IMVS,CELL}(\omega) = -\frac{V_{CELL,AC}(\omega,t)}{q_e \Sigma_{AC}(\omega,t)} \tag{2.21}$$

Chapter 3

Experimental

All experiments were performed at one sun with Zahner TLS03 CIMPS QE/IPCE tuneable light source. The software used for measurements and analyzing methods is Zahner Thales Z3.04 USB.

The setup of the measurements can be seen in Figure 3.1 and a simplified flow chart of the system is presented in Figure 3.2. The cell is mounted on an adjustable surface where height and angle can be adjusted by nano screws in addition to the distance from the light source. For all experiments the photo-electrode is connected as the working electrode. Furthermore, the setup consists of two potentiostats in order to control two different systems - one potentiostat to control the light source and one for the solar cell. Additionally all cells that are tested in this report consist of a TiO_2 substrate with $I_3^-/3\,I^-$-electrolyte, but with different dyes coated on the TiO_2-surface. All measurements are performed with three samples for each of the solar cells with the different dyes with both reference electrode and counter electrode connected to the TCO at the back of the solar cell.

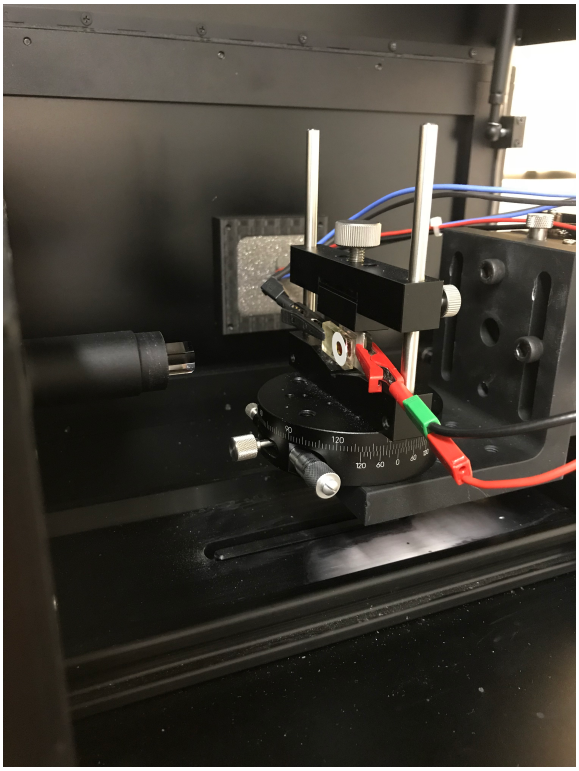

Figure 3.1: Physical setup of the system. The cell is mounted on the adjustable surface and the electrodes are connected. The black and blue electrode is the test electrode and the red and green electrode is the referance and counter electrode connected together. The crystal to the left is the light source.

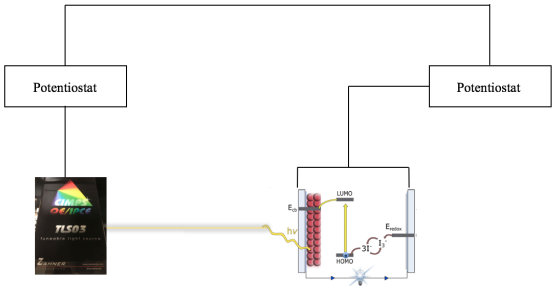

Figure 3.2: Flowchart of the experimental setup. Two potentiostats are connected in series controlling the Zahner TLS03 CIMPS QE/IPCE tuneable light source and the cell.

3.1 DSSC fabrication

The cell fabrication was performed with the help of PhD candidate Audun Formo Buene at the department of chemistry at NTNU. Below is a description of the dye fabrication, based on the information recieved by Audun Buene et al.[4].

TEC-8 FTO glass was washed with Deconex 21 (2 g/L H_2O) in an ultrasonic bath for 45 minutes, and then rinsed with deionized water and ethanol. The FTO glass was then air dryed before further cleaning was done in a UV-ozone cleaner for 15 minutes. A blocking layer was then deposited by immersion of the FTO glass in an aqueous solution of $TiCl_4$ (40 mM) for 30 minutes at 70 C, rinsing with deionized water and ethanol followed by another immersion for 30 minutes in an aqueous solution of $TiCl_4$ (40 mM) at 70 C, then rinsing with deionized water and ethanol.

Five layers of transparent TiO_2 paste were screen printed on the FTO glass (mesh count 250, active area 0.238 cm2), where the electrodes were heated to 125 C for 2-3 minutes between each layer. Finally, a scattering layer was screen printed, and the electrodes were sintered at 500 C for 30 minutes. The thickness of the sintered TiO_2 was measured to 17.5 μm (12.5 μm + 5 μm) with a profilometer. The electrodes were then post treated with $TiCl_4$ using the same conditions as previously described for 30 minutes.

The counter electrodes were fabricated by drilling holes in the FTO glass with a diamond drill bit. The catalytic Pt layer was deposited by dropcasting a 10 mM solution of H_2PtCl_6 in 2-propanol (5 $\mu L/cm2$), followed by firing at 400 C for 15 minutes.

The electrodes were annealed with a hot air gun at 480 C for 25 minutes before staining from a 0.5 mM solution in ethanol. The electrodes were stained for 20 hours, then rinsed in acetonitrile for 2 minutes and dried under N_2 flow. The cells were then sealed with a 25 μm Surlyn (Solaronix) gasket, melted with a 50 W PTC heat element for 3 20 seconds per cell.

The electrolyte was made following a procedure from Demadrille et al. [14], containing 0.5 M 1-butyl-3-methylimidazolium iodide, 0.1 M lithium iodide, 0.05 M I2 and 0.5 M tert-butylpyridine in acetonitrile. The electrolyte was injected by vacuum backfilling and the filling hole was sealed with Surlyn and a circular glass cover slip. The contacts for the anode and cathode were then painted with a conductive silver paint.

3.2 IV-characteristics

The IV-characteristics were mostly performed with a scan speed of $10\ \mathrm{mV\ s^{-1}}$. Some cells were tested with a scan speed of $100\ \mathrm{mV\ s^{-1}}$, but dynamic effects occurred at such a high scan speed, as was mentioned in subsection 2.3.1. This resulted in all IV-measurements to be performed at a scan speed of $10\ \mathrm{mV\ s^{-1}}$. The applied light intensity for all parallels was $37.8\ \mathrm{W/m^2}$ with wavelength $541\ \mathrm{nm}$.

3.3 Electrochemical impedance spectroscopy

During all the electrochemical impedance spectroscopy measurements the applied AC signal was $5\ \mathrm{mV}$ and the frequency range was varied between $100\ \mathrm{kHz}$ and $100\ \mathrm{mHz}$. The

wavelength of the incident light was $541\ \mathrm{nm}$ for all parallells at 50 % of max light intensity of the light source. This corresponds to a light intensity of $37.8\ \mathrm{W/m^2}$. The measurements were fitted in Matlab by the use of an objective function described by Mark E. Orazem and Bernard Tribollet[19] and equation (2.10). The full Matlab code is given in the Appendix. The parameters was then calculated from the relations of equations (2.11) through (2.15)

3.4 Intensity modulated photo-current spectroscopy

All the IMPS measurements were performed with an applied AC signal of $10\ \mathrm{mV\ s^{-1}}$ at potentiostatic control at short circuit current, meaning $E = 0V$, where the frequency range was varied between $100\ \mathrm{kHz}$ and $100\ \mathrm{mHz}$. Furthermore, the wavelength of the incident light was $541\ \mathrm{nm}$ for cells with N719-dye, $421\ \mathrm{nm}$ for cells with AFB-18-dye, $453\ \mathrm{nm}$ for cells with AFB-19-dye and $385\ \mathrm{nm}$ for cells with AFB-21-dye at 50 % of max light intensity of the light source. The chosen wavelengths correspond to the highest peaks of the four dyes absorption specters. However, the peak wavelengths of the absorption specters do not completely correspond to the wavelength used in the measurements due to discrete wavelengths of the diodes in the light source. In order to maintain pseudo linearity, only small intensity amplitudes were applied.

Chapter 4

Results

The results obtained for the measurements as well as calculated results will be presented in this section. The results are divided into subsections dependent on the dye on the DSSCs. A description of the the results and the most vital notes are stated in the paragraphs above the corresponding results.

4.1 N719

4.1.1 IV-characteristics

The IV-characteristics of the three different cells with N719 dye can be seen in Figure 4.1. Experimental parameters from the measurements are shown in the yellow boxes in the respective figures. From the figures it can be seen that the reproducibility is very high with V_{oc} ranging from -0.511 V to -0.512 V, FF ranging from 0.815 to 0.817 and I_{sc} ranging from 20.26 µA to 20.61 µA.

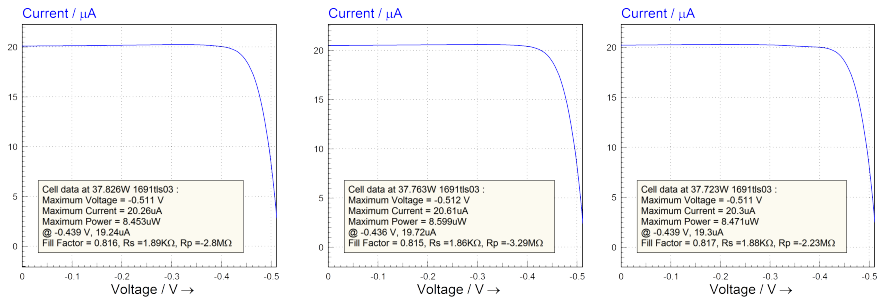

(a) Sample 1 **(b)** Sample 2 **(c)** Sample 3

Figure 4.1: IV-characteristics of three parallels of DSSCs consisting of a TiO_2 substrate, a $I_3^-/3\,I^-$-electrolyte and N719-dye at scan rate 10mV/s. The incident light had an intensity of $37.8\ \mathrm{W/m^2}$ with a wavelength of $541\ \mathrm{nm}$.

Below, the most important values from the IV-measurements for cells with N719-dye are tabulated in Table 4.1. The power conversion efficiency, PCE, is calculated by use of Equation (2.1).

Table 4.1: Summary of results for IV-characteristics for N719-dye.

Parameter [Unit]	N719-1	N719-2	N719-3
V_{oc} [V]	-0.511	-0.512	-0.511
I_{sc} [µA]	20.26	20.61	20.30
P_{max} [µW]	8.453	8.599	8.471
FF [-]	0.816	0.815	0.817
PCE [%]	5.31	5.41	5.33

4.1.2 Electrochemical Impedance Spectroscopy

The results for electrochemical impedance spectroscopy of the three cells with N719 dye can be seen in Figure 4.2, 4.4, 4.6, 4.3, 4.5 and 4.7. Along with the IV-measurements the EIS-measurements show a high reproducibility as the phase angle peaks at $0.3\ \mathrm{mHz}$ and at $15\ \mathrm{Hz}$ for all parallels as can be seen in the bode-plots. Similarly the modulus of impedance for all the three parallels show the same behaviour where the slope of the curve flattens out at frequencies higher than $3\ \mathrm{kHz}$. From the figures 4.3b, 4.5b and 4.7b it can be seen that the modeled results do not fit accurately to the experimental results as the fitted curve (blue dotted line) follow the shape in Figure 2.10b, while the experimental curve (red line) follow the shape in Figure 2.10c. The fitted results suggests that $\omega_3 < \omega_L$, although the experimental results seemingly suggests that $\omega_3 > \omega_L$.

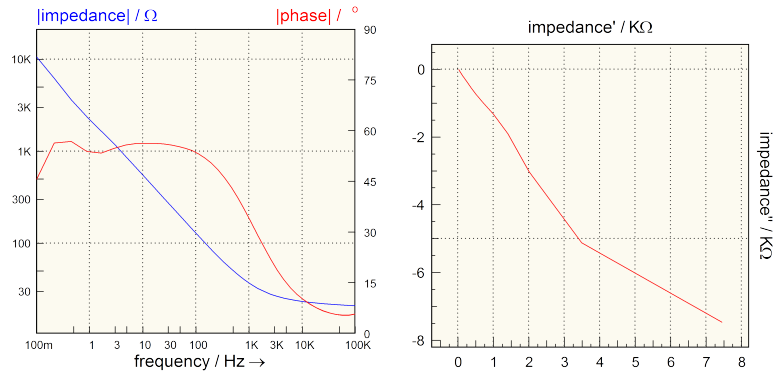

(a) Bode-plot. **(b)** Nyquist-plot.

Figure 4.2: EIS of a DSSC consisting of a TiO_2 substrate, $I_3^-/3\,I^-$-electrolyte and N719-dye, sample 1. The measurement is performed at a potential of -0.439 V with incident light at a wavelength of 541 nm and an intensity of $37.8\ \mathrm{W/m^2}$. The results are represented in a Bode-plot and a Nyquist-plot.

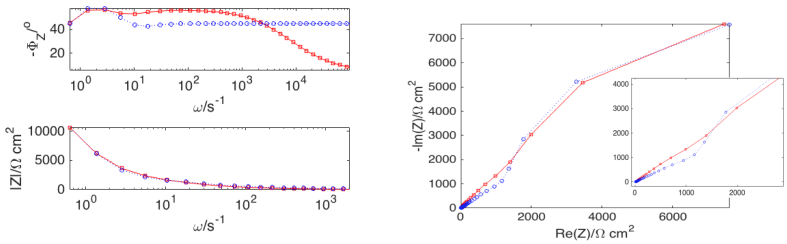

(a) Bode plot. **(b)** Nyquist-plot.

Figure 4.3: EIS of a DSSC consisting of a TiO_2 substrate, $I_3^-/3\,I^-$-electrolyte and N719-dye, sample 1. The measurement is performed at a potential of -0.439 V with incident light at a wavelength of 541 nm and an intensity of $37.8\ \mathrm{W/m^2}$. The results are represented in a Bode-plot and a Nyquist-plot, where the red line represents the experimental values and the blue dotted line represents the fitted values modeled with the use of the equivalent circuit in Figure 2.9.

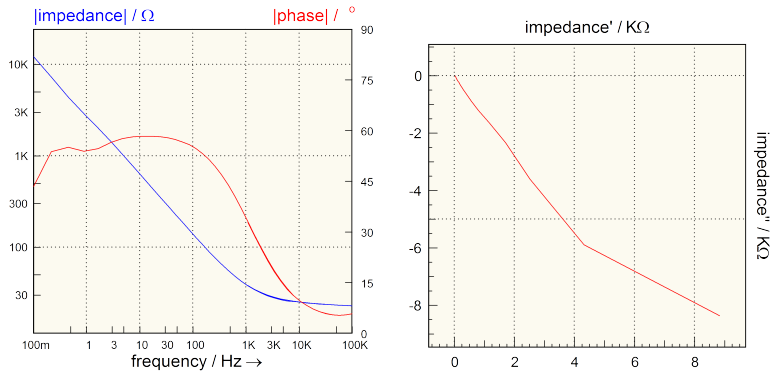

(a) Bode-plot. **(b)** Nyquist-plot.

Figure 4.4: EIS of a DSSC consisting of a TiO_2 substrate, $I_3^-/3\,I^-$-electrolyte and N719-dye, sample 2. The measurement is performed at a potential of -0.436 V with incident light at a wavelength of 541 nm and an intensity of $37.8\ \mathrm{W/m^2}$. The results are represented in a Bode-plot and a Nyquist-plot.

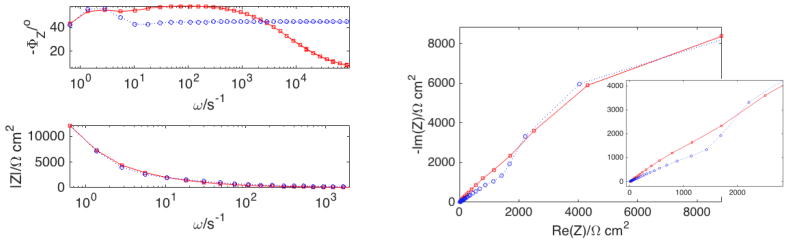

(a) Bode plot. **(b)** Nyquist-plot.

Figure 4.5: EIS of a DSSC consisting of a TiO_2 substrate, $I_3^-/3\,I^-$-electrolyte and N719-dye, sample 2. The measurement is performed at a potential of -0.436 V with incident light at a wavelength of 541 nm and an intensity of $37.8\ \mathrm{W/m^2}$. The results are represented in a Bode-plot and a Nyquist-plot, where the red line represents the experimental values and the blue dotted line represents the fitted values modeled with the use of the equivalent circuit in Figure 2.9.

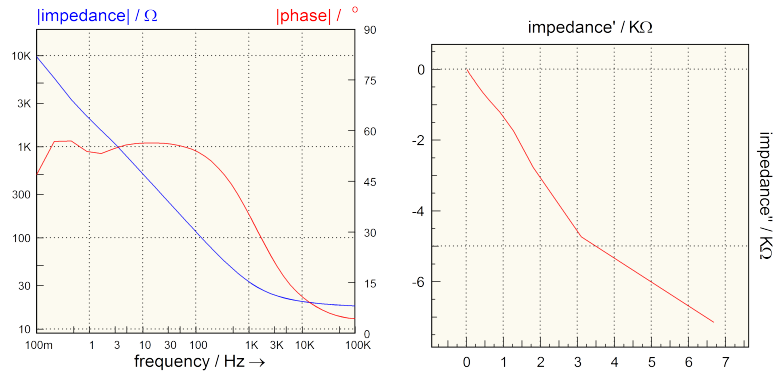

(a) Bode-plot. **(b)** Nyquist-plot.

Figure 4.6: EIS of a DSSC consisting of a TiO_2 substrate, $I_3^-/3\,I^-$-electrolyte and N719-dye, sample 3. The measurement is performed at a potential of -0.439 V with incident light at a wavelength of 541 nm and an intensity of $37.8\ \mathrm{W/m^2}$. The results are represented in a Bode-plot and a Nyquist-plot.

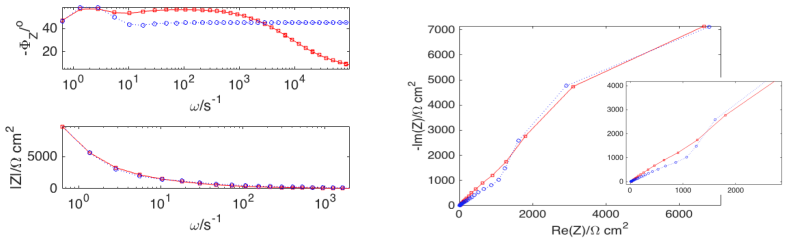

(a) Bode plot. **(b)** Nyquist-plot.

Figure 4.7: EIS of a DSSC consisting of a TiO_2 substrate, $I_3^-/3\,I^-$-electrolyte and N719-dye, sample 3. The measurement is performed at a potential of -0.439 V with incident light at a wavelength of 541 nm and an intensity of $37.8\ \mathrm{W/m^2}$. The results are represented in a Bode-plot and a Nyquist-plot, where the red line represents the experimental values and the blue dotted line represents the fitted values modeled with the use of the equivalent circuit in Figure 2.9.

The calculated values obtained from the EIS-measurements for cells with N719-dye are tabulated in Table 4.2 below. The values are calculated by use of equations 2.11 through 2.15.

Table 4.2: Calculated results for EIS-measurements for cells with N719-dye.

Parameter [Unit]	**N719-1**	**N719-2**	**N719-3**
τ_{rec} [s]	2.000	1.667	2.000
τ_{trans} [s]	0.476	0.526	0.500
L [µm]	35.86	31.14	35.00
D [$\mu m^2/s$]	643	581	613
c_μ [m/s]	1578	1776	1493
η_{cc} [-]	0.76	0.68	0.75

4.1.3 Intensity Modulated Photocurrent Spectroscopy

Also for IMPS the cells with N719-dye show high reproducibilty. The modulus of photocurrent have bottom points at approximately $460\ \mathrm{Hz}$ for all three samples with corresponding photocurrent ranging from $14\ \mathrm{nAW^{-1}m^2}$ in sample 1 to $10\ \mathrm{nAW^{-1}m^2}$ in sample 3. The behaviour of the modulus of the photocurrent and the phase angle are similar for all samples both at high and low frequencies as can be seen in Figure 4.8a, 4.9a and 4.10a.

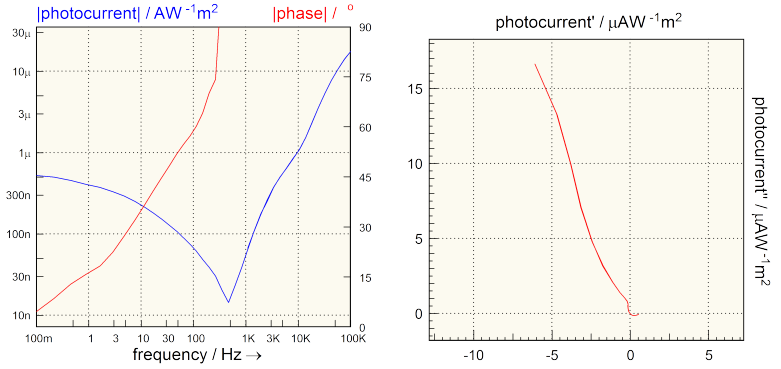

(a) Bode-plot. **(b)** Nyquist-plot.

Figure 4.8: IMPS of a DSSC consisting of a TiO_2 substrate, $I_3^-/3\,I^-$-electrolyte and N719-dye, sample 1. The measurement is performed at short circuit current ($E = 0\ \mathrm{V}$) with incident light at a wavelength of $541\ \mathrm{nm}$ and an intensity of $37.8\ \mathrm{W/m^2}$. The results are represented in a Bode-plot and a Nyquist-plot.

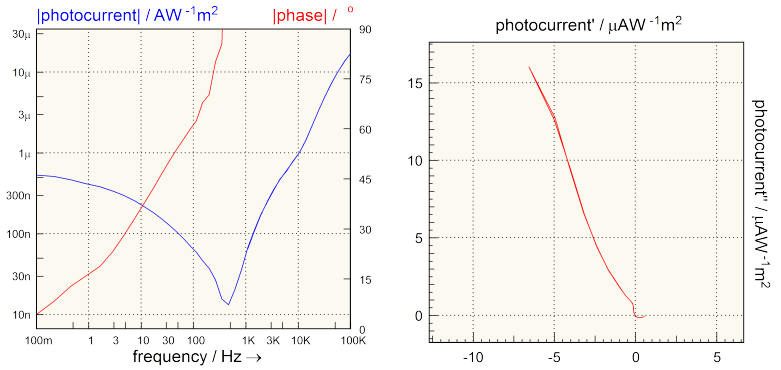

(a) Bode-plot. **(b)** Nyquist-plot.

Figure 4.9: IMPS of a DSSC consisting of a TiO_2 substrate, $I_3^-/3\,I^-$-electrolyte and N719-dye, sample 2. The measurement is performed at short circuit current ($E = 0\ \mathrm{V}$) with incident light at a wavelength of $541\ \mathrm{nm}$ and an intensity of $37.8\ \mathrm{W/m^2}$. The results are represented in a Bode-plot and a Nyquist-plot.

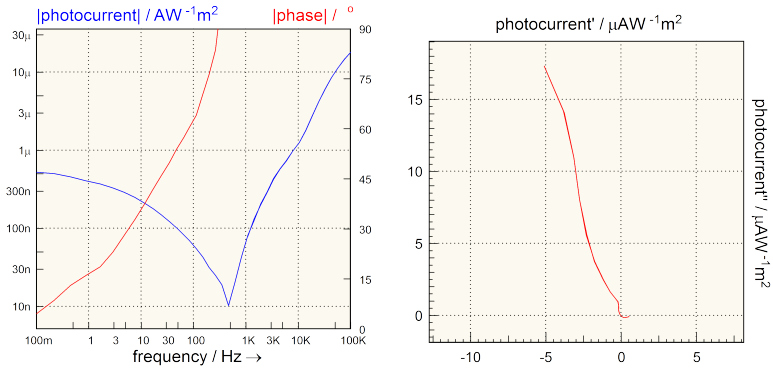

(a) Bode-plot. **(b)** Nyquist-plot.

Figure 4.10: IMPS of a DSSC consisting of a TiO_2 substrate, $I_3^-/3\,I^-$-electrolyte and N719-dye, sample 3. The measurement is performed at short circuit current (E = 0 V) with incident light at a wavelength of $541\ \mathrm{nm}$ and an intensity of $37.8\ \mathrm{W/m^2}$. The results are represented in a Bode-plot and a Nyquist-plot.

The calculated values obtained from the IMPS-measurements for cells with N719-dye are tabulated in Table 4.3 below. The values are calculated by use of equations 2.18 and 2.19.

Table 4.3: Calculated results of IMPS-measurements for cells with N719-dye.

Parameter [Unit]	**N719-1**	**N719-2**	**N719-3**
f_{IMPS} [1/s]	461.7	461.7	461.7
τ_{trans} [µs]	344.89	344.89	344.89
D [µm/s^2]	0.38	0.38	0.38

4.2 AFB-18

4.2.1 IV-characteristics

The current-voltage-characteristics for DSSCs with AFB-18 dye showed high reproducibility, which can be seen in figure 4.11. The V_{oc} range from -0.581 V to -0.586 V in sample 1 and 3 respectively whereas the I_{sc} range from 26.85 µA in sample 3 to 28.07 µA in sample 2, and the resulting FF range from 0.793 to 0.796. When compared to the IV-characteristics for cells with N719-dye in figure 4.1, it can be seen that V_{oc}, I_{sc} and P_max are higher for all parallels with AFB-18 dye than for the parallels with N719-dye, but the FF is lower. This can be explained by the relations from equation 2.6, where the FF increases with increased P_max and decreases with increased V_{oc} and I_{sc}.

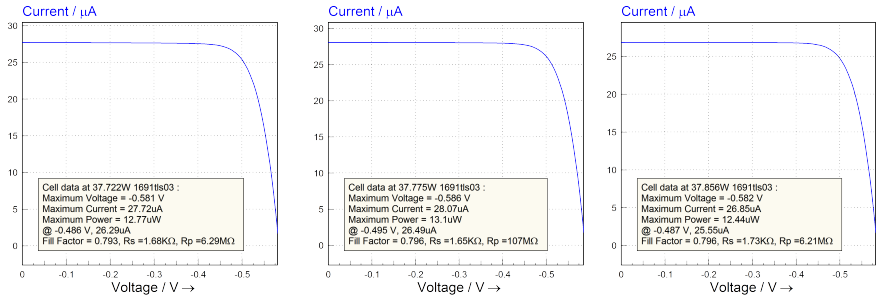

(a) Sample 1 **(b)** Sample 2 **(c)** Sample 3

Figure 4.11: IV-characteristics of three parallels of DSSCs consisting of a TiO_2 substrate, $I_3^-/3\,I^-$-electrolyte and AFB-18-dye at scan rate 10mV/s. The incident light had an intensity of $37.8\ \mathrm{W/m^2}$ with a wavelength of $541\ \mathrm{nm}$.

Below, the most important values from the IV-measurements for cells with AFB-18-dye are tabulated in Table 4.4. The power conversion efficiency, PCE, is calculated by use of Equation (2.1).

Table 4.4: Summary of results for IV-characteristics for AFB18-dye.

Parameter [Unit]	AFB18-1	AFB18-2	AFB18-3
V_{oc} [V]	-0.581	-0.586	-0.582
I_{sc} [µA]	27.72	28.07	26.85
P_{max} [µW]	12.77	13.1	12.44
FF [-]	0.793	0.796	0.796
PCE [%]	8.03	8.23	7.82

4.2.2 Electrochemical Impedance Spectroscopy

For the EIS-measurements for cells with AFB-18-dye, sample 1 showed a very different behaviour than sample 2 and 3, which can be seen in figures 4.12 through 4.16. For sample 1 the phase angle peaks at two frequencies; at 3 Hz and at 450 Hz. For sample 2 and 3 the results were very similar, with three peaks for the phase angle present at 3 Hz, at 50 Hz and at 900 Hz. Notice how both the modeled results and the experimental results in the Nyquist-plots for sample 1 in Figure 4.13b both follow the shape in Figure 2.10b. This is not the case for sample 2 and 3 in Figures 4.15b and 4.17b, as the fitted curve (blue dotted line) follow the shape in Figure 2.10b, while the experimental curve (red line) follow the shape in Figure 2.10c.

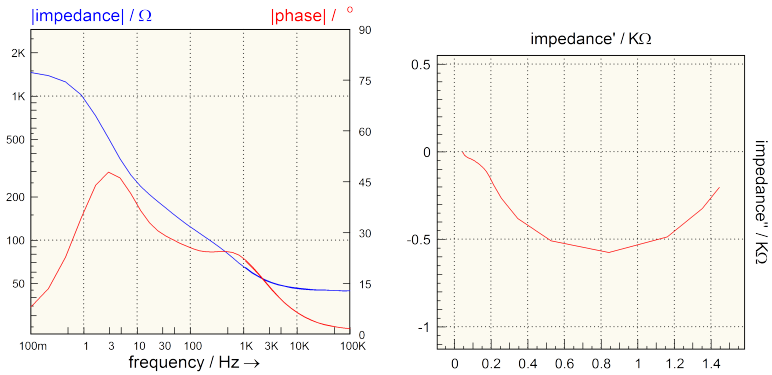

(a) Bode-plot. **(b)** Nyquist-plot.

Figure 4.12: EIS of a DSSC consisting of a TiO_2 substrate, $I_3^-/3\,I^-$-electrolyte and AFB-18-dye, sample 1. The measurement is performed at a potential of -0.486 V with incident light at a wavelength of 541 nm and an intensity of $37.8\ \mathrm{W/m^2}$. The results are represented in a Bode-plot and a Nyquist-plot.

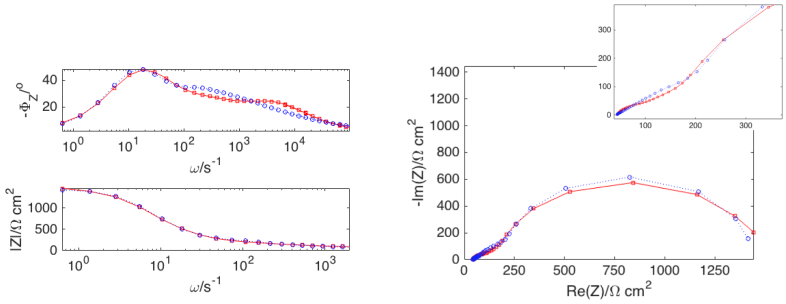

(a) Bode plot. **(b)** Nyquist-plot.

Figure 4.13: EIS of a DSSC consisting of a TiO_2 substrate, $I_3^-/3\,I^-$-electrolyte and AFB-18-dye, sample 1. The measurement is performed at a potential of -0.486 V with incident light at a wavelength of 541 nm and an intensity of $37.8\ \mathrm{W/m^2}$. The results are represented in a Bode-plot and a Nyquist-plot, where the red line represents the experimental values and the blue dotted line represents the fitted values modeled with the use of the equivalent circuit in Figure 2.9.

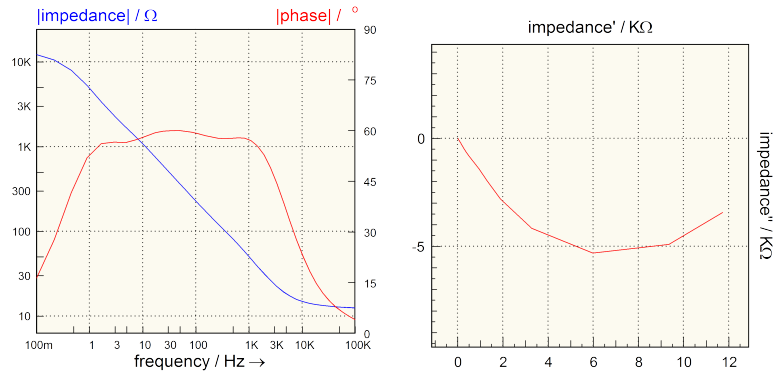

(a) Bode-plot. **(b)** Nyquist-plot.

Figure 4.14: EIS of a DSSC consisting of a TiO_2 substrate, $I_3^-/3\,I^-$-electrolyte and AFB-18-dye, sample 2. The measurement is performed at a potential of -0.495 V with incident light at a wavelength of 541 nm and an intensity of $37.8\ \mathrm{W/m^2}$. The results are represented in a Bode-plot and a Nyquist-plot.

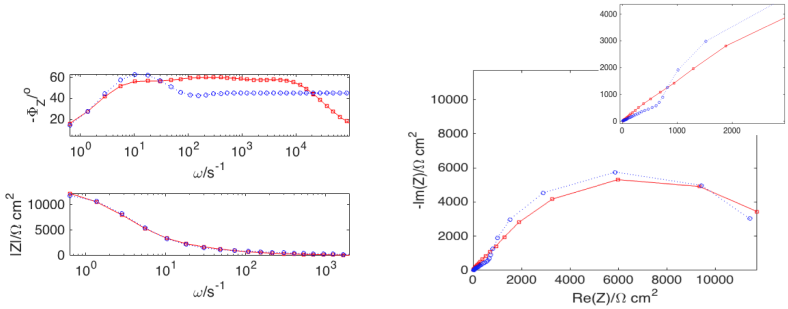

(a) Bode plot. **(b)** Nyquist-plot.

Figure 4.15: EIS of a DSSC consisting of a TiO_2 substrate, $I_3^-/3\,I^-$-electrolyte and AFB-18-dye, sample 2. The measurement is performed at a potential of -0.495 V with incident light at a wavelength of 541 nm and an intensity of $37.8\ \mathrm{W/m^2}$. The results are represented in a Bode-plot and a Nyquist-plot, where the red line represents the experimental values and the blue dotted line represents the fitted values modeled with the use of the equivalent circuit in Figure 2.9.

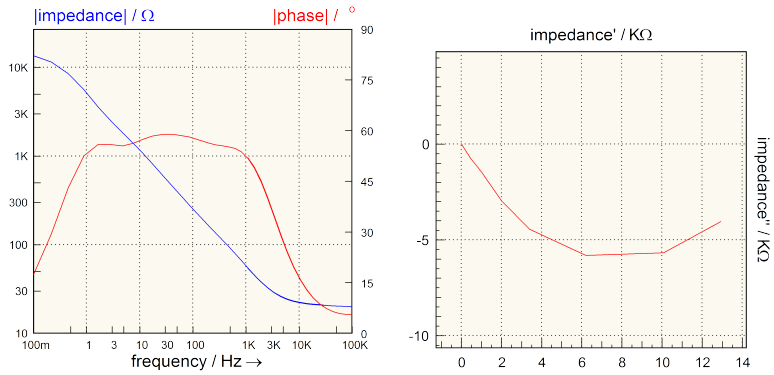

(a) Bode-plot. **(b)** Nyquist-plot.

Figure 4.16: EIS of a DSSC consisting of a TiO_2 substrate, $I_3^-/3\,I^-$-electrolyte and AFB-18-dye, sample 3. The measurement is performed at a potential of -0.486 V with incident light at a wavelength of 541 nm and an intensity of $37.8\ \mathrm{W/m^2}$. The results are represented in a Bode-plot and a Nyquist-plot.

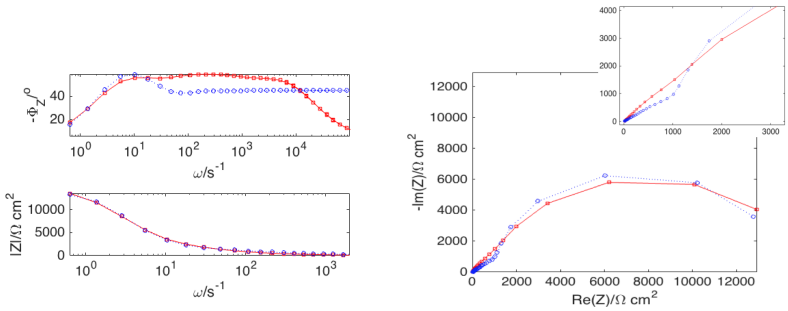

(a) Bode plot. **(b)** Nyquist-plot.

Figure 4.17: EIS of a DSSC consisting of a TiO_2 substrate, $I_3^-/3\,I^-$-electrolyte and AFB-18-dye, sample 3. The measurement is performed at a potential of -0.486 V with incident light at a wavelength of 541 nm and an intensity of $37.8\ \mathrm{W/m^2}$. The results are represented in a Bode-plot and a Nyquist-plot, where the red line represents the experimental values and the blue dotted line represents the fitted values modeled with the use of the equivalent circuit in Figure 2.9.

The calculated values obtained from the EIS-measurements for cells with AFB-18-dye are tabulated in Table 4.5 below. The values are calculated by use of equations 2.11 through 2.15.

Table 4.5: Calculated results for EIS-measurements for cells with AFB-18-dye.

Parameter [Unit]	**AFB-18-1**	**AFB-18-2**	**AFB-18-3**
τ_{rec} [s]	0.179	0.400	0.455
τ_{trans} [s]	0.072	0.091	0.109
L [µm]	26.82	34.09	33.32
D [$\mu m^2/s$]	4020	2905	2442
c_μ [m/s]	4238	6404	5922
η_{cc} [-]	0.60	0.77	0.76

4.2.3 Intensity Modulated Photocurrent Spectroscopy

In the measurements for IMPS for DSSCs with AFB-18-dye, all samples experienced the same behaviour for the photocurrent at low frequencies (< 1 kHz), which can be seen from figures 4.18a, 4.19a and 4.20a. However, at higher frequencies sample 1 deviates from sample 2 and 3 as the photocurrent does not peak at all, whereas for sample 2 and 3 it peaks at 5 kHz.

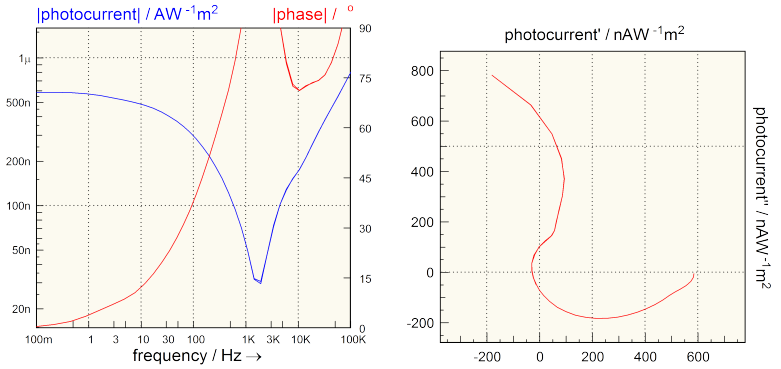

(a) Bode-plot. **(b)** Nyquist-plot.

Figure 4.18: IMPS of a DSSC consisting of a TiO_2 substrate, $I_3^-/3\,I^-$-electrolyte and AFB-18-dye, sample 1. The measurement is performed at short circuit current ($E = 0$ V) with incident light at a wavelength of 421 nm and an intensity of 88.4 W/m^2. The results are represented in a Bode-plot and a Nyquist-plot.

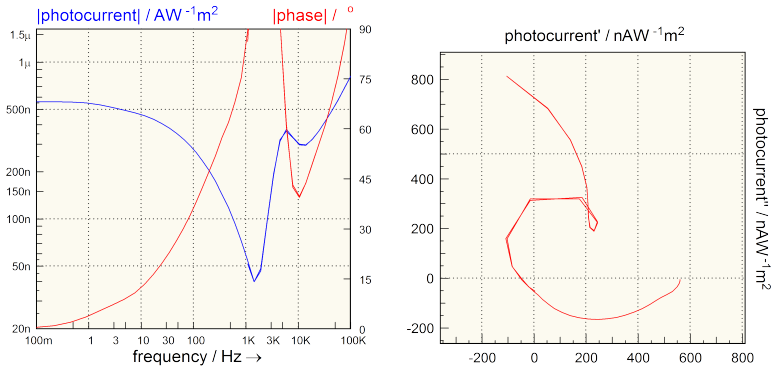

(a) Bode-plot. **(b)** Nyquist-plot.

Figure 4.19: IMPS of a DSSC consisting of a TiO_2 substrate, $I_3^-/3\,I^-$-electrolyte and AFB-18-dye, sample 2. The measurement is performed at short circuit current ($E = 0$ V) with incident light at a wavelength of 421 nm and an intensity of 88.8 W/m^2. The results are represented in a Bode-plot and a Nyquist-plot.

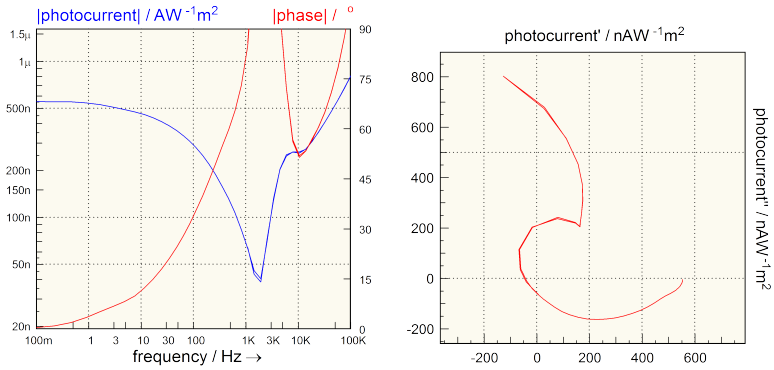

(a) Bode-plot. **(b)** Nyquist-plot.

Figure 4.20: IMPS of a DSSC consisting of a TiO_2 substrate, $I_3^-/3\,I^-$-electrolyte and AFB-18-dye, sample 3. The measurement is performed at short circuit current (E $=0$ V) with incident light at a wavelength of 421 nm and an intensity of 88.9 W/m^2. The results are represented in a Bode-plot and a Nyquist-plot.

The calculated values obtained from the IMPS-measurements for cells with AFB-18-dye are tabulated in Table 4.6 below. The values are calculated by use of equations 2.18 and 2.19.

Table 4.6: Calculated results of IMPS-measurements for cells with AFB-18-dye.

Parameter [Unit]	AFB-18-1	AFB-18-2	AFB-18-3
f_{IMPS} [1/s]	1901.0	1432.4	1901.0
τ_{trans} [µs]	83.76	111.17	83.76
D [µm/s^2]	1.56	1.17	1.56

4.3 AFB-19

4.3.1 IV-characteristics

The results for the current-voltage-measurements for DSSCs with AFB-19-dye are displayed in figure 4.21. The measured V_{oc} was higher than for cells with N719- and AFB-18-dye, with values from -0.615 V in sample 1 to -0.631 V in sample 3. The highest current measured of cells with AFB-19-dye was comparable to the equivalent results of cells with AFB-18-dye (see figure 4.11), with I_{sc} for cells with AFB-18 ranging from 27.21 µA in sample 3 to 27.21 µA in sample 2, compared to the range from 26.85 µA to 28.07 µA for cells with AFB-18-dye.

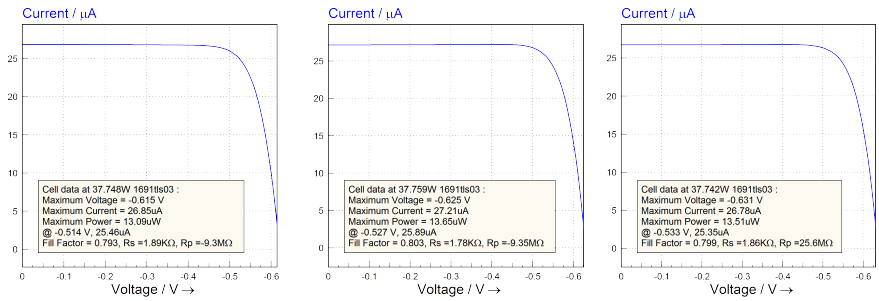

(a) Sample 1 **(b)** Sample 2 **(c)** Sample 3

Figure 4.21: IV-characteristics of three parallels of DSSCs consisting of a TiO_2 substrate, $I_3^-/3\,I^-$-electrolyte and AFB-19-dye at scan rate 10mV/s. The incident light had an intensity of $37.8\ \mathrm{W/m^2}$ with a wavelength of $541\ \mathrm{nm}$.

Below, the most important values from the IV-measurements for cells with AFB-19-dye are tabulated in Table 4.7. The power conversion efficiency, PCE, is calculated by use of Equation (2.1).

Table 4.7: Summary of results for IV-characteristics for AFB19-dye.

Parameter [Unit]	AFB19-1	AFB19-2	AFB19-3
V_{oc} [V]	-0.615	-0.625	-0.631
I_{sc} [µA]	26.85	27.21	26.78
P_{max} [µW]	13.09	13.65	13.51
FF [-]	0.793	0.803	0.799
PCE [%]	8.24	8.59	8.49

4.3.2 Electrochemical Impedance Spectroscopy

The EIS-measurements for cells with AFB-19-dye displayed a high reproducibility. The phase angle peaks at 2 kHz and at 30 kHz for all samples, which can be seen from the Bode-plots in figures 4.22a, 4.24a and 4.26a. In addition the Nyquist-plots for all parallels follow the shape where $\omega_3 < \omega_L$, described by Bisquert et al. from Figure 2.10b, both for the fitted curve and the experimental curve, as can be seen in Figures 4.23b, 4.25b and 4.27b.

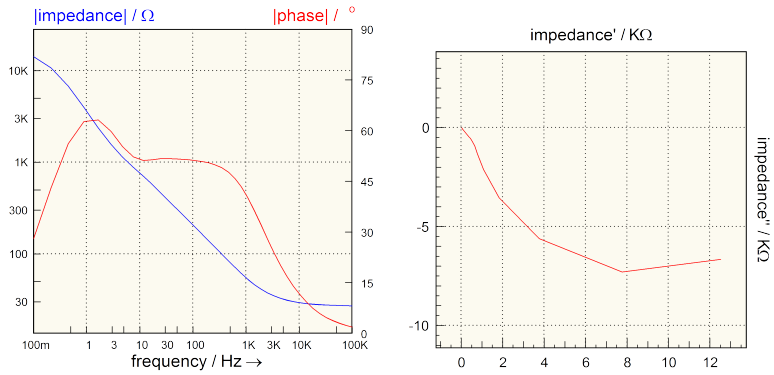

(a) Bode-plot. **(b)** Nyquist-plot.

Figure 4.22: EIS of a DSSC consisting of a TiO_2 substrate, $I_3^-/3\,I^-$-electrolyte and AFB-19-dye, sample 1. The measurement is performed at a potential of -0.514 V with incident light at a wavelength of 541 nm and an intensity of $37.8\ \mathrm{W/m^2}$. The results are represented in a Bode-plot and a Nyquist-plot.

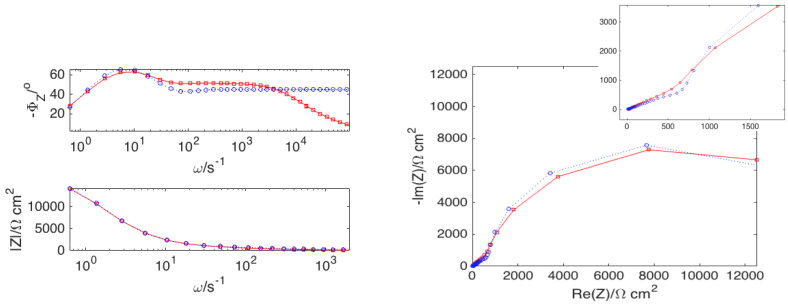

(a) Bode plot. **(b)** Nyquist-plot.

Figure 4.23: EIS of a DSSC consisting of a TiO_2 substrate, $I_3^-/3\,I^-$-electrolyte and AFB-19-dye, sample 1. The measurement is performed at a potential of -0.514 V with incident light at a wavelength of 541 nm and an intensity of $37.8\ \mathrm{W/m^2}$. The results are represented in a Bode-plot and a Nyquist-plot, where the red line represents the experimental values and the blue dotted line represents the fitted values modeled with the use of the equivalent circuit in Figure 2.9.

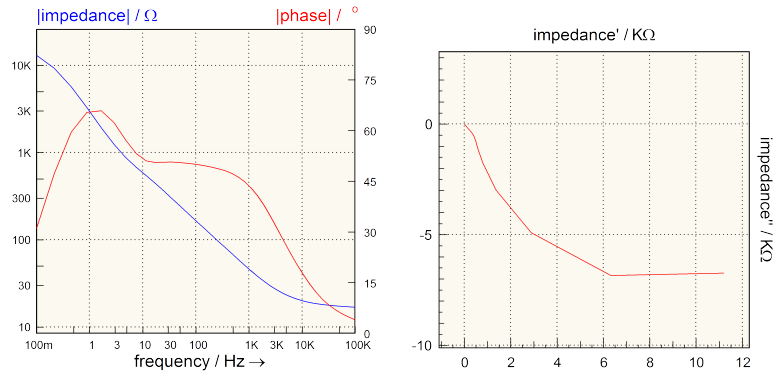

(a) Bode-plot. **(b)** Nyquist-plot.

Figure 4.24: EIS of a DSSC consisting of a TiO_2 substrate, $I_3^-/3\,I^-$-electrolyte and AFB-19-dye, sample 2. The measurement is performed at a potential of -0.525 V with incident light at a wavelength of 541 nm and an intensity of $37.8\ \mathrm{W/m^2}$. The results are represented in a Bode-plot and a Nyquist-plot.

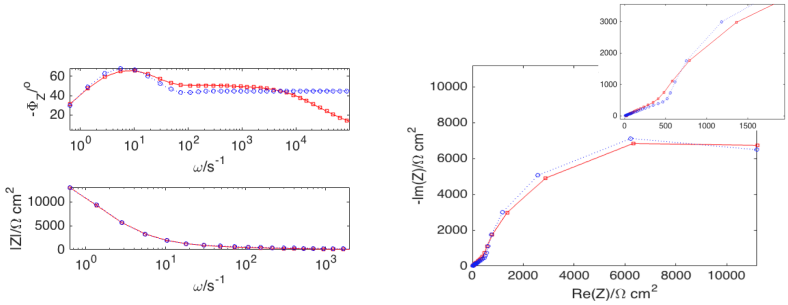

(a) Bode plot. **(b)** Nyquist-plot.

Figure 4.25: EIS of a DSSC consisting of a TiO_2 substrate, $I_3^-/3\,I^-$-electrolyte and AFB-19-dye, sample 2. The measurement is performed at a potential of -0.525 V with incident light at a wavelength of 541 nm and an intensity of $37.8\ \mathrm{W/m^2}$. The results are represented in a Bode-plot and a Nyquist-plot, where the red line represents the experimental values and the blue dotted line represents the fitted values modeled with the use of the equivalent circuit in Figure 2.9.

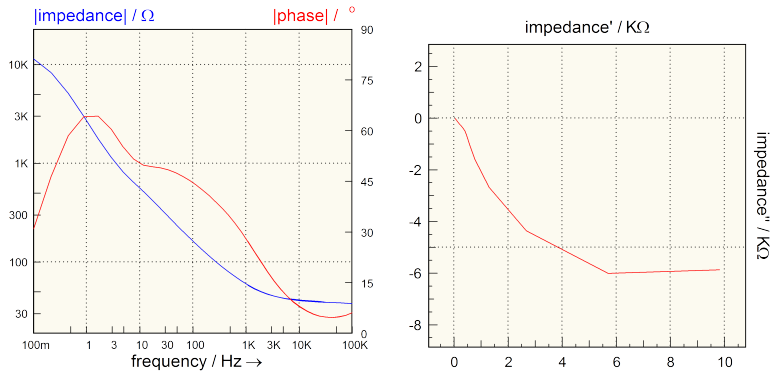

(a) Bode-plot. **(b)** Nyquist-plot.

Figure 4.26: EIS of a DSSC consisting of a TiO_2 substrate, $I_3^-/3\,I^-$-electrolyte and AFB-19-dye, sample 3. The measurement is performed at a potential of -0.533 V with incident light at a wavelength of 541 nm and an intensity of $37.8\ \mathrm{W/m^2}$. The results are represented in a Bode-plot and a Nyquist-plot.

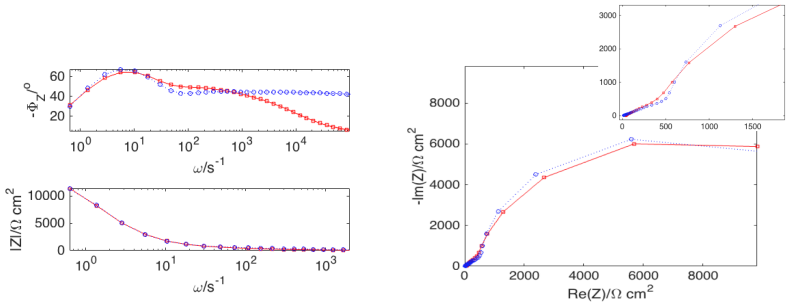

(a) Bode plot. **(b)** Nyquist-plot.

Figure 4.27: EIS of a DSSC consisting of a TiO_2 substrate, $I_3^-/3\,I^-$-electrolyte and AFB-19-dye, sample 3. The measurement is performed at a potential of -0.533 V with incident light at a wavelength of 541 nm and an intensity of $37.8\ \mathrm{W/m^2}$. The results are represented in a Bode-plot and a Nyquist-plot, where the red line represents the experimental values and the blue dotted line represents the fitted values modeled with the use of the equivalent circuit in Figure 2.9.

The calculated values obtained from the EIS-measurements for cells with AFB-19-dye are tabulated in Table 4.8 below. The values are calculated by use of equations 2.11 through 2.15.

Table 4.8: Calculated results for EIS-measurements for cells with AFB-19-dye.

Parameter [Unit]	AFB-19-1	AFB-19-2	AFB-19-3
τ_{rec} [s]	0.833	0.909	0.909
τ_{trans} [s]	0.100	0.092	0.099
L [µm]	45.44	49.12	47.46
D [$\mu m^2/s$]	2477	2654	2478
c_μ [m/s]	4136	3791	3517
η_{cc} [-]	0.88	0.90	0.89

4.3.3 Intensity Modulated Photocurrent Spectroscopy

The three samples of DSSCs with AFB-19-dye all display photocurrents of 690 $\mathrm{nAW^{-1}m^2}$ at 100 mHz with bottom points at 2 kHz. It is peculiar how the phase angles in sample 1 and 3 show the shape of $f(x) = -x^2$ at frequencies > 3 kHz and not for sample 2.

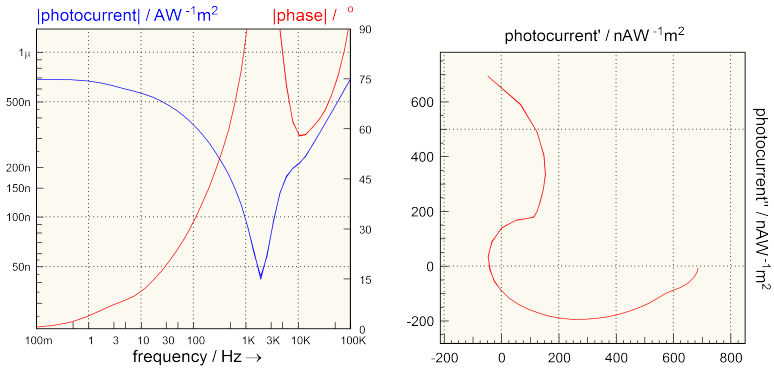

(a) Bode-plot. **(b)** Nyquist-plot.

Figure 4.28: IMPS of a DSSC consisting of a TiO_2 substrate, $I_3^-/3\,I^-$-electrolyte and AFB-19-dye, sample 1. The measurement is performed at short circuit current (E = 0 V) with incident light at a wavelength of 453 nm and an intensity of 93.7 $\mathrm{W/m^2}$. The results are represented in a Bode-plot and a Nyquist-plot.

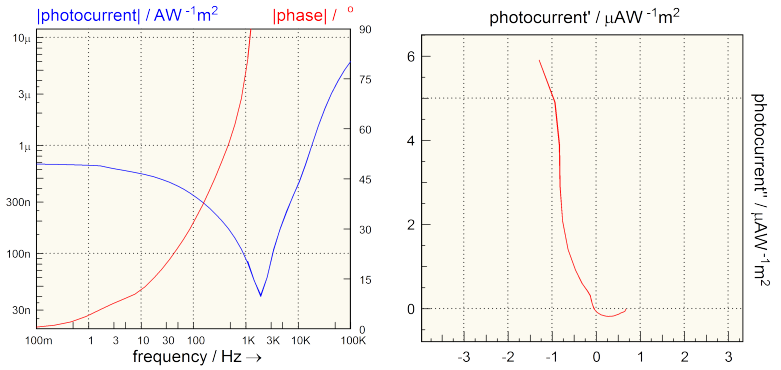

(a) Bode-plot. **(b)** Nyquist-plot.

Figure 4.29: IMPS of a DSSC consisting of a TiO_2 substrate, $I_3^-/3\,I^-$-electrolyte and AFB-19-dye, sample 2. The measurement is performed at short circuit current ($E = 0$ V) with incident light at a wavelength of 453 nm and an intensity of 93.7 W/m^2. The results are represented in a Bode-plot and a Nyquist-plot.

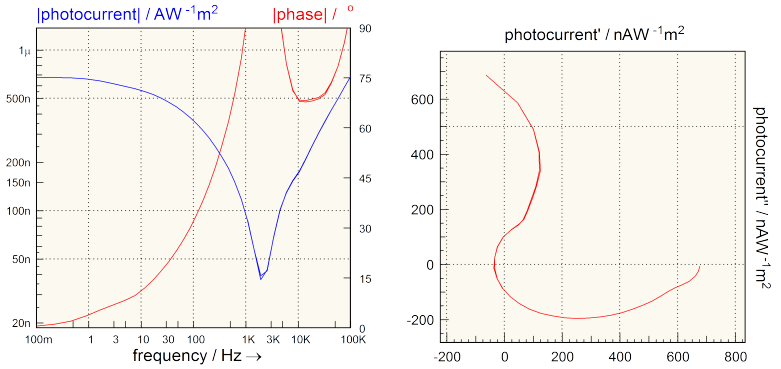

(a) Bode-plot. **(b)** Nyquist-plot.

Figure 4.30: IMPS of a DSSC consisting of a TiO_2 substrate, $I_3^-/3\,I^-$-electrolyte and AFB-19-dye, sample 3. The measurement is performed at short circuit current ($E = 0$ V) with incident light at a wavelength of 453 nm and an intensity of 93.9 W/m^2. The results are represented in a Bode-plot and a Nyquist-plot.

The calculated values obtained from the IMPS-measurements for cells with AFB-19-dye are tabulated in Table 4.9 below. The values are calculated by use of equations 2.18 and 2.19.

Table 4.9: Calculated results of IMPS-measurements for cells with AFB-19-dye.

Parameter [Unit]	AFB-19-1	AFB-19-2	AFB-19-3
f_{IMPS} [1/s]	1901.0	1901.0	1901.0
τ_{trans} [µs]	83.76	83.76	83.76
D [µm/s^2]	1.56	1.56	1.56

4.4 AFB-21

4.4.1 IV-characteristics

The IV-characteristics for cells with AFB-21-dye showed great promise. With V_{oc} ranging from -0.641 V in sample 3 to -0.658 V in sample 3, I_{sc} ranging from 28.80 µA in sample 3 to 30.24 µA in sample 1 and FF ranging from 0.821 in sample 3 to 0.826 in sample 2, the measured values are higher at all the above-mentioned parameters than for all other parallels with N719-, AFB-18- and AFB-19-dye.

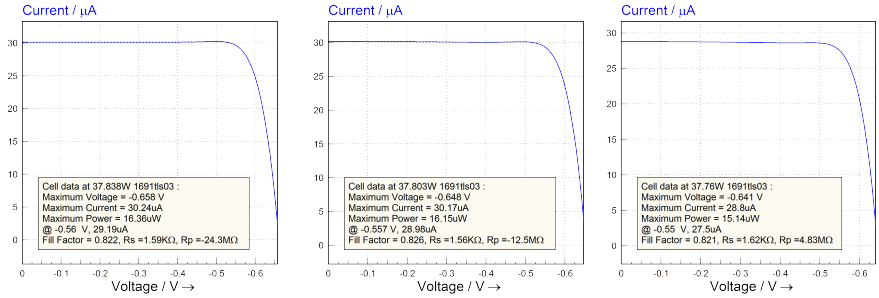

(a) Sample 1 **(b)** Sample 2 **(c)** Sample 3

Figure 4.31: IV-characteristics of three parallels of DSSCs consisting of a TiO_2 substrate, $I_3^-/3\,I^-$-electrolyte and AFB-21-dye at scan rate 10mV/s. The incident light had an intensity of 37.8 W/m^2 with a wavelength of 541 nm.

Below, the most important values from the IV-measurements for cells with AFB-21-dye are tabulated in Table 4.10. The power conversion efficiency, PCE, is calculated by use of Equation (2.1).

Table 4.10: Summary of results for IV-characteristics for AFB21-dye.

Parameter [Unit]	AFB21-1	AFB21-2	AFB21-3
V_{oc} [V]	-0.658	-0.648	-0.641
I_{sc} [µA]	30.24	30.17	28.8
P_{max} [µW]	16.36	16.15	15.14
FF [-]	0.822	0.826	0.821
PCE [%]	10.29	10.16	9.53

4.4.2 Electrochemical Impedance Spectroscopy

The EIS measurements for cells with AFB-21-dye shows peaks for the phase angles at 1 kHz. For sample 1 the phase angle dramatically increases for frequencies > 10 kHz. The Nyquist-plots for all parallels follow the shape where $\omega_3 < \omega_L$, described by Bisquert et al. from Figure 2.10b, both for the fitted curve and the experimental curve, as can be seen in Figures 4.33b, 4.35b and 4.37b.

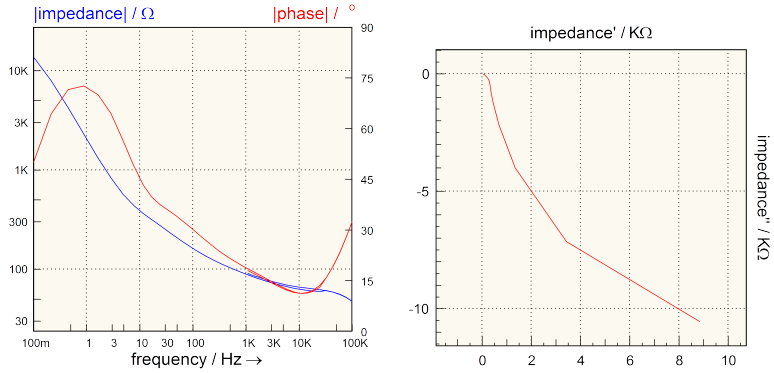

(a) Bode-plot. **(b)** Nyquist-plot.

Figure 4.32: EIS of a DSSC consisting of a TiO_2 substrate, $I_3^-/3\,I^-$-electrolyte and AFB-21-dye, sample 1. The measurement is performed at a potential of -0.561 V with incident light at a wavelength of 541 nm and an intensity of $37.8\ \mathrm{W/m^2}$. The results are represented in a Bode-plot and a Nyquist-plot.

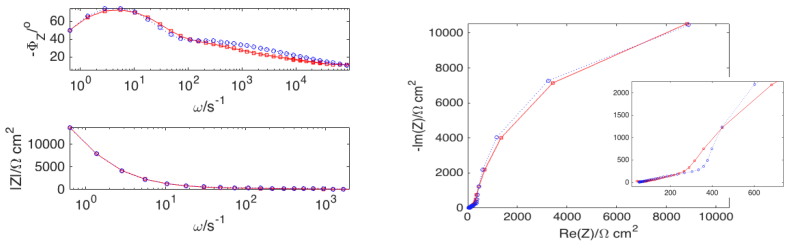

(a) Bode plot. **(b)** Nyquist-plot.

Figure 4.33: EIS of a DSSC consisting of a TiO_2 substrate, $I_3^-/3\,I^-$-electrolyte and AFB-21-dye, sample 1. The measurement is performed at a potential of -0.561 V with incident light at a wavelength of 541 nm and an intensity of $37.8\ \mathrm{W/m^2}$. The results are represented in a Bode-plot and a Nyquist-plot, where the red line represents the experimental values and the blue dotted line represents the fitted values modeled with the use of the equivalent circuit in Figure 2.9.

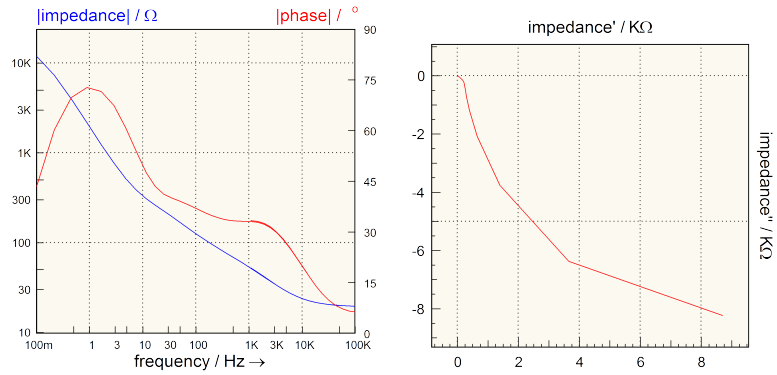

(a) Bode-plot. **(b)** Nyquist-plot.

Figure 4.34: EIS of a DSSC consisting of a TiO_2 substrate, $I_3^-/3\,I^-$-electrolyte and AFB-21-dye, sample 2. The measurement is performed at a potential of -0.557 V with incident light at a wavelength of 541 nm and an intensity of $37.8\ \mathrm{W/m^2}$. The results are represented in a Bode-plot and a Nyquist-plot.

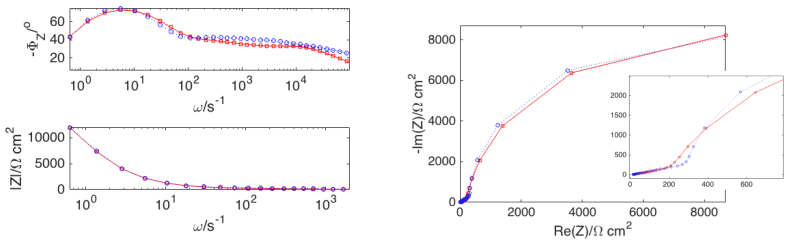

(a) Bode plot. **(b)** Nyquist-plot.

Figure 4.35: EIS of a DSSC consisting of a TiO_2 substrate, $I_3^-/3\,I^-$-electrolyte and AFB-21-dye, sample 2. The measurement is performed at a potential of -0.557 V with incident light at a wavelength of 541 nm and an intensity of $37.8\ \mathrm{W/m^2}$. The results are represented in a Bode-plot and a Nyquist-plot, where the red line represents the experimental values and the blue dotted line represents the fitted values modeled with the use of the equivalent circuit in Figure 2.9.

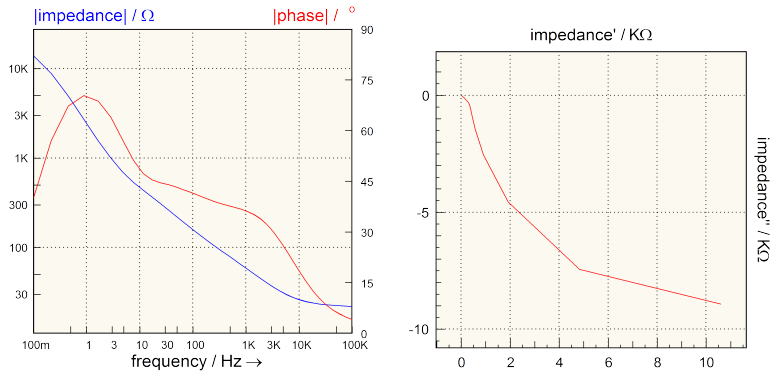

(a) Bode-plot. **(b)** Nyquist-plot.

Figure 4.36: EIS of a DSSC consisting of a TiO_2 substrate, $I_3^-/3\,I^-$-electrolyte and AFB-19-dye, sample 3. The measurement is performed at a potential of -0.550 V with incident light at a wavelength of 541 nm and an intensity of $37.8\ \mathrm{W/m^2}$. The results are represented in a Bode-plot and a Nyquist-plot.

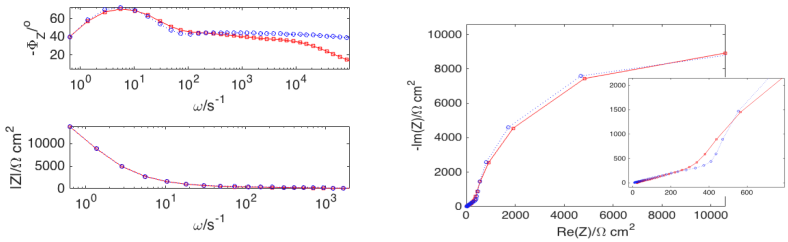

(a) Bode plot. **(b)** Nyquist-plot.

Figure 4.37: EIS of a DSSC consisting of a TiO_2 substrate, $I_3^-/3\,I^-$-electrolyte and AFB-21-dye, sample 3. The measurement is performed at a potential of -0.550 V with incident light at a wavelength of 541 nm and an intensity of $37.8\ \mathrm{W/m^2}$. The results are represented in a Bode-plot and a Nyquist-plot, where the red line represents the experimental values and the blue dotted line represents the fitted values modeled with the use of the equivalent circuit in Figure 2.9.

The calculated values obtained from the EIS-measurements for cells with AFB-21-dye are tabulated in Table 4.11 below. The values are calculated by use of equations 2.11 through 2.15.

Table 4.11: Calculated results for EIS-measurements for cells with AFB-21-dye.

Parameter [Unit]	AFB-21-1	AFB-21-2	AFB-21-3
τ_{rec} [s]	2.000	1.429	1.429
τ_{trans} [s]	0.078	0.071	0.087
L [µm]	75.30	78.54	61.67
D [$\mu m^2/s$]	2834	4318	2662
c_μ [m/s]	2559	3373	2999
η_{cc} [-]	0.96	0.95	0.94

4.4.3 Intensity Modulated Photocurrent Spectroscopy

The IMPS results for DSSCs with AFB-21-dye displays a similar behaviour as the equivalent results for DSSCs with AFB-18-dye: all samples experiences the same behaviour for the photocurrent at low frequencies (< 1 kHz), which can be seen from figures 4.38a, 4.39a and 4.40a. However, at higher frequencies sample 1 deviates from sample 2 and 3 as the photocurrent does not peak at all, whereas for sample 2 and 3 it peaks at 5 kHz.

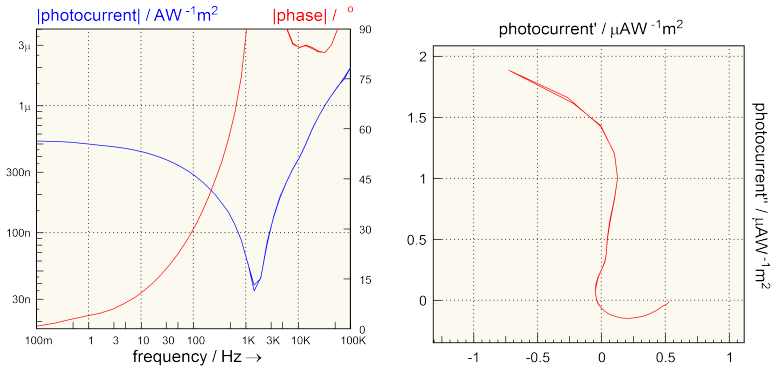

(a) Bode-plot. **(b)** Nyquist-plot.

Figure 4.38: IMPS of a DSSC consisting of a TiO_2 substrate, $I_3^-/3\,I^-$-electrolyte and AFB-21-dye, sample 1. The measurement is performed at short circuit current (E = 0 V) with incident light at a wavelength of 385 nm and an intensity of 25.8 W/m^2. The results are represented in a Bode-plot and a Nyquist-plot.

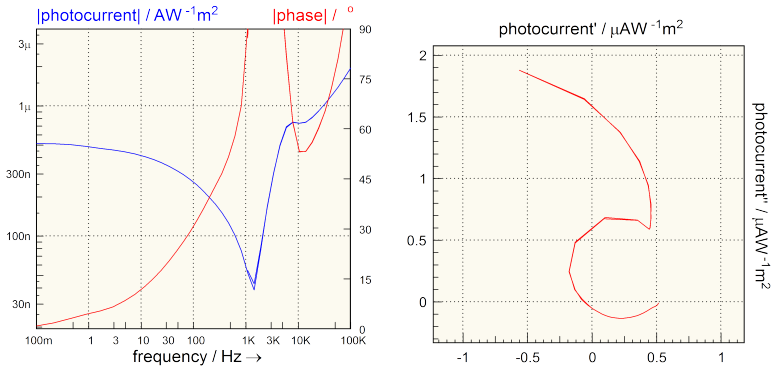

(a) Bode-plot. **(b)** Nyquist-plot.

Figure 4.39: IMPS of a DSSC consisting of a TiO_2 substrate, $I_3^-/3\,I^-$-electrolyte and AFB-21-dye, sample 2. The measurement is performed at short circuit current ($E = 0$ V) with incident light at a wavelength of 385 nm and an intensity of $25.8\ \mathrm{W/m^2}$. The results are represented in a Bode-plot and a Nyquist-plot.

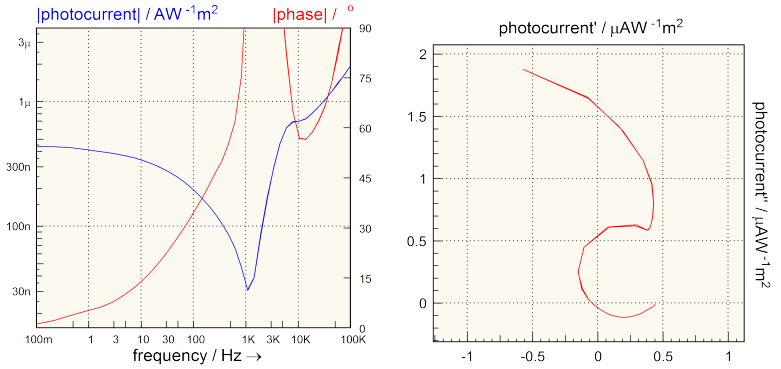

(a) Bode-plot. **(b)** Nyquist-plot.

Figure 4.40: IMPS of a DSSC consisting of a TiO_2 substrate, $I_3^-/3\,I^-$-electrolyte and AFB-21-dye, sample 3. The measurement is performed at short circuit current ($E = 0$ V) with incident light at a wavelength of 385 nm and an intensity of $25.8\ \mathrm{W/m^2}$. The results are represented in a Bode-plot and a Nyquist-plot.

The calculated values obtained from the IMPS-measurements for cells with AFB-21-dye are tabulated in Table 4.12 below. The values are calculated by use of equations 2.18 and 2.19.

Table 4.12: Calculated results of IMPS-measurements for cells with AFB-21-dye.

Parameter [Unit]	**AFB-21-1**	**AFB-21-2**	**AFB-21-3**
f_{IMPS} [1/s]	1432.4	1432.4	1079.2
τ_{trans} [µs]	111.17	111.17	147.55
D [µm/s^2]	1.17	1.17	0.88

Chapter 5

Discussion

5.1 Discussion of sources of error

The measured results show reproducibility to a high extent. This can be exemplified by the following results for the IV-characteristics of cells with AFB-21-dye, which obtained the biggest deviation: V_{oc} ranging from -0.641 V in sample 3 to -0.658 V in sample 3, I_{sc} ranging from 28.80 µA in sample 3 to 30.24 µA in sample 1 and FF ranging from 0.821 in sample 3 to 0.826 in sample 2. This means that both the DSSC-fabrication and the experiments are performed accurately and has a high reliability. One exception to this is sample 1 of DSSC with AFB-18-dye, which has a very different behavior in the EIS-measurements than the two other parallels with the same dye. This is also the case at high frequencies in the IMPS-measurements.

The modeled results for the cells with AFB-19-dye, AFB-21-dye and for sample 1 with AFB-18-dye are accurate both at high and low frequencies. For cells with N719-dye and sample 2 and 3 with AFB-18-dye the results are not equally accurate at intermediate and high frequencies. In section 2.3.2 is it stated that it is expected that the modeled EIS results are good at low frequencies, which is true based on the modeled Bode-plots. For more accurate results at intermediate and high frequencies, the model should account for the capacitance at the counter electrode, the bulk resistance and the electron transport in the electrolyte, described by Nernst diffusion as done by Kern et al.[8].

The modeled Nyquist-plot suggests a curve equal to Figure 2.11b, where $\omega_3 < \omega_L$ for the cells with N719-dye and sample 2 and 3 for cells with AFB18-dye. Based on the shape of the experimental curve, ω_3 should be $> \omega_L$ in accordance with Bisquert et al. [7]. However, the shape of the Bode-plots for cells with N719-dye and sample 2 and 3 with AFB-18-dye suggests three time constants for describing the cell. The peak at the lowest frequency is expected to represent the frequency where electron transport in the electrolyte, described by Nernst diffusion, is dominating. The peak at intermediate frequency represents the frequency where the impedance of the electron transport and of recombination in the TiO_2 is dominating. The peak at the highest frequency represents the frequency where the capacitance at the counter electrode and the bulk resistance dominates. Another

explanation could be that for the scenarios where $\omega_3 > \omega_L$ Bisquert et al. [7] proposes a different relation for the electrode impedance than the one used in this work.

5.2 Discussion of results

From Figure 2.7 it can be seen that the AFB-18, AFB-19 and AFB-21 display a stronger and broader absorption spectra in the visible area and high infrared area than N719, which correlates well with the higher I_{sc} obtained in the IV-characteristics. From the tables 4.11, 4.21 and 4.31 it can be seen that the cells with AFB-21-dye is measured to have a higher I_{sc} than the cells with AFB-19-dye, which in turn is measured to be higher than the cells with AFB-18-dye. Based on the absorption spectra obtained, this seems reasonable.

In all the three different pure organic dyes, LUMO is located at the anchoring group whereas HOMO has another spatial position in order to enhance the performance of the cell. This reduces the recombination, as the tunneling distances for recombination back to the HOMO of the dye are decidedly longer than for charge injection from the LUMO, meaning that the injection is kinetically favored. However, the explanation of why there are differences in the time constants for recombination for the respective cells is of organic chemists to answer.

All cells with the pure organic dyes have a higher PCE compared to the cells with the organo-metallic dye N719. The cells with AFB-18-dye, AFB-19-dye and AFB-21 dye are measured to have an average PCE of 8.03%, 8.44% and 9.99% respectively, while the cells with N719-dye is measured to an average of 5.35%.

The calculated results for the EIS-measurements can be seen in Tables 4.2, 4.5, 4.8 and 4.11. The time constants for transport, τ_{trans}, are very equal for the cells with the pure organic dyes, ranging from 0.071 s in sample 2 with AFB-21-dye to 0.109 s in sample 3 with AFB-18-dye. For the cells with N719-dye the lowest obtained τ_{trans} is 0.476 s. This means that the average collection of electrons in the cells with AFB-18, AFB-19 and AFB-21 dyes are 4-7 times faster than for the cells with N719. This is an important reason why the cells with the pure organic dyes have a higher PCE.

The small differences in the time constants for transport means that there must be bigger differences in the time constants for recombination, in order to explain the differences in the IV-characteristics for the cells with the pure organic dyes through τ_{trans} and τ_{rec}. τ_{rec} range from 0.179 s to 0.455 s, from 0.833 s to 0.909 s and from 1.427 s to 2.000 s for cells with AFB-18-dye, AFB-19-dye and AFB-21 dye respectively. This means that the process of recombination is approximately 2 times slower for cells with AFB-21-dye than the cells with AFB-19-dye, and 3-11 times slower than the cells with AFB-18-dye. This is probably the main reason why $PCE_{AFB-21} > PCE_{AFB-19} > PCE_{AFB-18}$, where the subindex is the dye used in the cell. For the cells with N719-dye the time constants for recombination is the highest obtained, ranging from 1.667 s to 2.000 s, which partially compensate for the slow average collection in the cells.

For all the cells the effective diffusion length, L, was greater than the film thickness, d, which was an assumption made in order to obtain equation 2.4. L $>$ d means in practice that the electrons can be efficiently collected at the electrode before they recombine [12]. Cells with AFB-21-dye obtained the highest effective diffusion lengths with an average of 71.83 µm, whereas the cells with AFB-18-dye, AFB-19-dye and N719-dye obtained

an average of 31.41 µm, 47.34 µm and 34.00 µm respectively. This substantiates the reasoning why the cells with AFB-21-dye has the highest performance. On the other hand it is noted that the effective diffusion length for cells with N719 are slightly higher than for the cells with AFB-18, although $\tau_t rans$ is significantly lower for cells with AFB-18-dye than for cell with N719-dye. From the relation in equation 2.11, this can be explained by significantly higher time constants for recombination for cells with N719-dye than for cells with AFB-18-dye.

For the time constants for transport calculated by the IMPS-measurements, the results seem implausible as the values are in the order of µs and the exact same results are obtained for many of the different samples across cells with different dyes. τ_{trans} for cells with N719 is 2-4 times as high as for the cells with the pure organic dyes, in contradiction with the results obtained from the EIS-measurements. From equation 2.11 the time constant for transport for EIS measurements, τ_{EIS}, can be expressed as

$$\tau_{EIS} = \frac{d^2}{D}, \tag{5.1}$$

knowing that $L = \sqrt{D\tau}$ and assuming $\beta = 1$. Similarly the time constant for transport for IMPS measurements can be expressed as as

$$\tau_{IMPS} = \frac{d^2}{2.35D}, \tag{5.2}$$

through the relation in equation 2.19. This means that the relation between τ_{imps} and τ_{eis} should be

$$\tau_{IMPS} = 0.4\tau_{EIS}. \tag{5.3}$$

This is not the case for the results obtained, where the relation is approximately $\tau_{IMPS} = 10^{-4}\tau_{EIS}$.

Chapter 6

Conclusion

Through current-voltage measurements, EIS measurements and IMPS measurements reproducible results are obtained. The IV-characteristics shows promise that pure organic dyes can compete with the commonly used Ruthenium complexes in terms of performance. All parallels for DSSCs with the pure organic dyes have a greater PCE than the cells with N719-dye. This is explained by the significantly lower τ_{trans} obtained for the cells with pure organic dyes than the for the cells with N719-dye. In other words, the average collection of electrons in the TiO_2 occur faster in the cells with pure organic dyes compared to the cells with N719-dye. The cells with AFB-21-dye were measured to have the fastest average collection, the greatest diffusion length and the second slowest average recombination time and are with an average PCE of 9.99%, the best performing cells. The experimental Nyquist-plots for cells with AFB-19-dye, AFB-21-dye and sample 1 with AFB-18-dye exhibit the behavior of the scenario where $\omega_3 < \omega_L$ from Figure 2.11, explained by Bisquert et al. [7]. On the other hand the cells with N719-dye and sample 1 and 2 with AFB-18-dye exhibit the behavior of the scenario where $\omega_3 > \omega_L$ from Figure 2.11c, which is notable.

The model used for fitting the EIS results is accurate at low frequencies, but shows signs of inaccuracy for intermediate and high frequencies. However, the obtained results are in the expected order and are reproducible and thus creates the foundation of the conclusion.

Further work ought to be expanded to a model that accounts for additional impedances occurring in the system, as done by Kern et al.[8]. This will expectedly provide more precise results than the model used in this work, as the it also takes into account the capacitance at the counter electrode, the bulk resistance and the electron transport in the electrolyte, described by Nernst diffusion. A possible equivalent circuit that could be implemented in such a model can be seen in Figure 2.10.

It was assumed that the transport was restricted to diffusion occurring in the TiO_2, leading to a hypothesis that the time constant for transport should be equal for all cells. The assessment of the cells shows that the hypothesis is valid for the DSSCs with the pure organic dyes, as the time constants for transport are very equal. In addition, through the

work in this thesis, it is shown that the IV-characteristics of solar cells can be explained through the corresponding time constants for transport and recombination.

Bibliography

[1] A. Hagfeldt, G. Boschloo, L. S., 2010. Dye-sensitized solar cells. Chem. Rev. 110 (11), 6595–6663.

[2] Abbott, D., 2010. Keeping the energy debate clean: How do we supply the world's energy needs? Proceedings of the IEEE 98 (1), 42–66.

[3] Archer, M. D., Nozik, A. J., 2008. Nanostructured and Photoelectrochemical Systems for Solar Photon Conversion. Imperial College Press.

[4] et al., A. B., 2018. Effect of -linkers on phenothiazine sensitizers for dye-sensitized solar cells. in submission.

[5] et al., D. G., 2012. Correlation between cell performance and physical transport parameters in dye solar cells. J. Phys. Chem. C 116 (1), 1151–1157.

[6] et al., H. Y., 2013. Band structure design of semiconductors for enhanced photocatalytic activity: The case of tio2. Progress in Natural Science: Materials International 23 (4), 402–407.

[7] et al., J. B., 2000. Doubling exponent models for the analysis of porous film electrodes by impedance. relaxation of tio2 nanoporous in aqueous solution. J. Phys. Chem. B 104, 2287–2298.

[8] et al., R. K., 2002. Modeling and interpretation of electrical impedance spectra of dye solar cells operated under open-circuit conditions. Electrochimica Acta 47 (-), 4213–4225.

[9] et al., S. S., 1994. Theoretical models for the action spectrum and the current-voltage characteristics of microporous semiconductor films in photoelectrochemical cells. J. Chem. Phys. 98, 5552–5556.

[10] Gerischer, H., 1978. Electrolytic decomposition and photodecomposition of compound semiconductors in contact with electrolytes. Journal of Vacuum Science and Technology 15, 1422.

[11] Halme, J., 2011. Linking optical and electrical small amplitude. Phys. Chem. Chem. Phys. 13, 12435–12446.

[12] Instruments, G., 2017. Dye solar cells part 3: Imps and imvs measurements. $https : //www.gamry.com/application - notes/physechem/dye - solar - cells - imps - imvs/$.

[13] IPCC, 2017. Renewable energy sources and climate change mitigation, special report of the intergovernmental panel on climate change, summary for policymakers and technical summary. $https : //www.ipcc.ch/pdf/special - reports/srren/SRREN_FD_SPM_final.pdf$.

[14] Joly D., Pellej L., N. S. O. F. C. J. C. J. N. e. a., 2014. A robust organic dye for dye sensitized solar cells based on iodine/iodide electrolytes combining high efficiency and outstanding stability. Sci. Rep 4 (-), 4033.

[15] Kruger, J. a., 2003. Charge transport and back reaction in solid-state-dye-sensitized solar cells: A study using intensity-modulated photovoltage and photocurrent spectroscopy. Journal of Physical Chemistry B 107, 7536–7539.

[16] Memming, 2000. Semiconductor Electrochemistry. Wiley-VCH, Weinheim.

[17] Morrison, S. R., 1980. Electrochemistry at Semiconductor and Oxidized Metal Electrodes. Plenum Press, New York.

[18] Nelson, J., 2003. The Physics of Solar Cells. Imperial College Press.

[19] Orazem, M. E., Tribollet, B., 2000. Electrochemical Impedance Spectroscopy. John Wiley and Sons, New Jersey.

Appendix

6.1 Matlab Code

6.1.1 Main Script

```
%Initialisation
clear all;
global w Zreal Zimag nmax pst

% CNLS = menu('Fit or plot','Fit','Plot');
CNLSfit = true;
% if CNLS==2
%     CNLSfit = false;
% end

% load data.txt data
load eis1kopi0981.txt data
data = eis1kopi0981;
display('Data loaded');
pst = 0.01;%Percent error assumed in the data

% Transfer data from file to internal memory used in CNLS.m.

k = 0;
dimok = true;

while dimok
    try
        k = k+1;
        w(k) = 2*pi()*data(k,2);
%         Zreal(k) = data(k,2);%Gamry format
%         Zimag(k) = data(k,3);%Gamry format
        Zmodulus(k) = data(k,3);%Zahner format
        PhaseAngle(k) = data(k,4);%Zahner format
        %Assumed to be the modulus of the impedance (Zahner)
        Zreal(k) = sqrt(Zmodulus(k)^2/(1+tand(PhaseAngle(k))^2));
        %Assumed to represent the phase angle (Zahner)
        Zimag(k) = Zreal(k)*tand(PhaseAngle(k));
    catch
        k = k - 1;
        dimok = false;
    end
end
```

```
% for ii=1:
%
% clear Zreal Zimag;
% for ii=1:

nmax = k;

%Calculate the complex capacitance
Zim = Zreal + j*Zimag;
Cap = 1./(j*w.*Zim);
% for ii=1:length(Zim)
%     Cap2(ii) = 1/(j*w(ii)*Zim(ii));
% end
% Cap - Cap2

maxz = max(max(Zreal),max(Zimag));
minz = min(min(Zreal),min(Zimag));
maxz = max(maxz,abs(minz));

%*************************************************************************
%
%LEVENBERG-MARQUARDT FIT TO DATA
%
%*************************************************************************

%Initial values for the fitted variables
x0 = [50 500 1000 100 0.09];

if CNLSfit

    %Lower bounds for variables:
    lb = zeros(size(x0));
    %Upper bounds on variables
    ub = 10.0*x0;%ones(size(x0));

    %Change the individual limits here if necessary.

    resnorm=10^20;
    residual=10^20;
    exitflag=100;
    %The Jacobian option is set to 'off' by default. Parameters for
    %nsqnonlin can be obtained by a call to optimget.

    options = optimset('TolFun',1e-8,'TolX',1e-8);             %Specification of tolerance
    %Fit and store data in x1. 'exitflag' should be 1 for a 100% successful fit
    [x1,resnorm,residual,exitflag]=lsqnonlin(@FCNLS,x0,lb,ub);
    if exitflag==1
        str = ['Exit flag: ' num2str(exitflag)];
        display(str);
    else
        str = ['Fit not 100 % successful. Exitflag: ' num2str(exitflag)];
        warndlg(str);
    end
    str = 'Fit result:';
    display(str);
    x1
end
```

```
%************************************************************************
%
%MAKE IMPEDANCE PLANE PLOT
%
%************************************************************************

for ii=1:length(w)
    if CNLSfit
        Zmod = Zmodel(x1,w(ii));
    else
        Zmod = Zmodel(x0,w(ii));
    end
    Cmod = 1/(j*w(ii)*Zmod);
    Zrmod(ii) = real(Zmod);
    Zimod(ii) = imag(Zmod);
    Crmod(ii) = real(Cmod);
    Cimod(ii) = imag(Cmod);
end

figure(1)
hold all
plot(Zreal,-Zimag,'-rs',Zrmod,-Zimod,':bo');
if minz < 0.0
    minz = -maxz;
else
    minz = 0.0;
end
axis([minz maxz minz maxz]);
%axis equal;
box on;
xlabel('Re(Z)/\Omega cm^{2}','FontSize',14)
ylabel('-Im(Z)/\Omega cm^{2}','FontSize',14)

%MAKE IMPEDANCE Bode PLOT
phi = -atand(Zimag./Zreal);           %Phase angle
modZ = sqrt((Zreal).^2 + (Zimag).^2); %Modulus
phimod = -atand(Zimod./Zrmod);           %Phase angle, model result
modZmod = sqrt((Zrmod).^2 + (Zimod).^2); %Modulus, model result

figure(2)
hold all
subplot(2,1,2);semilogx(w,modZ,'-rs',w,modZmod,':bo');
axis ([min(w) max(w) 0 max(modZ)]);
box on;
xlabel('\omega/s^{-1}','FontSize',14)
ylabel('|Z|/\Omega cm^{2}','FontSize',14)
hold all;
subplot(2,1,1);semilogx(w,phi,'-rs',w,phimod,':bo');
axis([min(w) max(w) min([phi phimod]) max([phi phimod])]);
box on;
xlabel('\omega/s^{-1}','FontSize',14)
ylabel('-\Phi_Z/^o','FontSize',14)
```

6.1.2 Supplementary Functions

```
function Z = Zmodel(x,omega)

    %CONSTANTS
    F = 96485.309;                  %Faraday number (C/mol)
    R = 8.31451;                    %Gas constant (J/molK)

    %MODEL PARAMETERS - ADD HERE
    T = 298;                        %Temperature, K, nominal value = 298

    %Fitting: Use the set of variables below
    R0= x(1);   %Series resistance in the electrochemical cell
    Z = R0;     %Initialization of the impedance model to the series resistance

    PreFactor = x(2);
    omega3 = x(3);
    omegaL = x(4);
    beta = x(5);                    %CPE exponent

%     Z = Z + PreFactor * 1/(sqrt(1+i*omega/omega3)) * \coth(sqrt(omega3/omegaL)*sqrt(1+i*
    Z = Z + PreFactor * 1/(sqrt(1+i*(omega/omega3)^beta)) * \coth(sqrt((omega3/omegaL)^bet

return


function F = FCNLS(x)
    global w Zreal Zimag nmax pst

    k=0;
    while k < nmax
        k=k+1;
        %Weighting:
        sigma = pst * sqrt(Zreal(k)^2 + Zimag(k)^2);
        sigma = 1.0;
        %Real part
        F(k) = Zreal(k) - real(Zmodel(x,w(k)));
        F(k) = F(k)/sigma;
        %Imaginary part
        F(nmax+k) = Zimag(k) - imag(Zmodel(x,w(k)));
        F(nmax+k) = F(nmax+k)/sigma;
    end

return


function F = FCNLS(x)
    global w Zreal Zimag nmax pst

    k=0;
    while k < nmax
        k=k+1;
        %Weighting:
        sigma = pst * sqrt(Zrdata(k)^2 + Zidata(k)^2);
        sigma = 1.0;
        %Real part
        F(k) = Zrdata(k) - real(Zmodel(x,w(k)));
        F(k) = F(k)/sigma;
        %Imaginary part
```

```
        F(nmax+k) = Zidata(k) - imag(Zmodel(x,w(k)));
        F(nmax+k) = F(nmax+k)/sigma;
    end

return
```